Fluid Dynamics Research

Lagrangian experiment and solution for irrotational finite-amplitude progressive gravity waves at uniform depth

To cite this article: Yang-Yih Chen *et al* 2010 *Fluid Dyn. Res.* **42** 045511

Fluid Dyn. Res. **42** (2010) 045511 (34pp) doi:10.1088/0169-5983/42/4/045511

Lagrangian experiment and solution for irrotational finite-amplitude progressive gravity waves at uniform depth

Yang-Yih Chen[1], **Hung-Chu Hsu**[2] **and Guan-Yu Chen**[3,4]

[1] Department of Marine Environment and Engineering, National Sun Yat-Sen Univeristy, Kaohsiung 804, Taiwan
[2] Research Center of Ocean Environment and Technology, National Cheng Kung University, Tainan 701, Taiwan
[3] Institute of Applied Marine Physics and Undersea Technology, National Sun Yat-Sen Univeristy, Kaohsiung 804, Taiwan

E-mail: yichen@mail.nsysu.edu.tw, hchsu@thl.ncku.edu.tw and guanyu@mail.nsysu.edu.tw

Received 23 November 2009, in final form 30 March 2010
Published 1 June 2010
Online at stacks.iop.org/FDR/42/045511

Communicated by M Funakoshi

Abstract
This study investigates the theory for predicting Lagrangian properties including particle orbit, Lagrangian mean level, Lagrangian wave frequency, mass transport velocity, wave profile, velocity distribution and wave pressure in progressive gravity water waves at uniform depth. A series of laboratory experiments are performed to measure the trajectories of particles and the wave pressure. Asymptotic solutions up to fifth order that describe irrotational finite amplitude progressive gravity water waves are derived in completely Lagrangian coordinates. The analytical Lagrangian solution that is uniformly valid satisfies the irrotational condition, the dynamic boundary condition and the zero pressure at the free surface. The explicit fifth-order parametric solution highlights the trajectory of a water particle and the wave kinematics above the mean water level and within a vertical water column, which were calculated previously by an approximation method using an Eulerian approach. Mass transport up to fourth order associated with a particle displacement can now be obtained directly in Lagrangian form. In particular, the Lagrangian wave frequency and the Lagrangian mean level of particle motion can also be obtained, which are different from those in an Eulerian description. By comparing the present fifth-order asymptotic solution with data from laboratory experiments, it is found that theoretical results show good agreement with experimental data.

(Some figures in this article are in colour only in the electronic version)

[4] Author to whom any correspondence should be addressed.

0169-5983/10/045511+34$30.00

1. Introduction

Fluid flow motion may be described either by observing the fluid velocity at fixed positions or by tracing particle trajectories along the flow. These alternative descriptions are called, respectively, the Eulerian and Lagrangian methods. For an incompressible fluid, the Eulerian approach is clearly preferable because the corresponding continuity equation is linear. It is known that the Eulerian description at the free surface is always expressed by a Taylor series at a fixed water level, which implicitly assumes that the surface profile is a differentiable single-valued function. This Taylor series expansion with respect to the free surface suggests the use of a perturbation method, and the first successful application was Stokes' wave theory (Stokes 1847, Johnson 1997). It provides a basis for regular asymptotic techniques with higher-order permanent wave solutions at uniform water depth or other practical applications (Skjelbreia and Hendrickson 1960, Cokelet 1977, Fenton 1985). Recent studies on Stokes waves with small or large amplitudes without performing approximations provide the qualitative features of the particle trajectories (Constantin 2001a, 2006, Constantin and Escher 2007).

In the Eulerian form, the wave surface is given as an implicit function, unlike the Lagrangian form, which is described with a parametric representation of the particle motion. The Lagrangian description is more appropriate for limiting free surface motion, but these features cannot be described by classical Eulerian solutions (Biesel 1952, Naciri and Mei 1993, Chen *et al* 2006, Chen and Hsu 2009a, 2009b, Constantin and Escher 2007). The first water wave theory in Lagrangian coordinates in which the flow possesses finite vorticity was presented by Gerstner (1802), and was re-discovered by Rankine (1863). Miche (1944) proposed perturbation Lagrangian solutions to the second order for a gravity wave. Pierson (1962) applied the Navier–Stokes equation to deep water waves in the Lagrangian formulae and obtained the first-order Lagrangian solution. Sanderson (1985) obtained second-order solutions for small-amplitude internal waves in a Lagrangian coordinate system. Constantin (2001b) considered first-order Lagrangian solutions for edge waves on a sloping beach. Buldakov *et al* (2006) developed a Lagrangian asymptotic formulation up to the fifth order for nonlinear water waves in deep water.

Chang *et al* (2007) followed Chen's third-order Lagrangian solutions (Chen 1994a, 1994b) to obtain the fifth-order Lagrangian solutions for a regular progressive wave in water with finite depth. However, Chang's solution is circuitous and not completely within the Lagrangian system because an additional condition with the surface elevation derived from the Eulerian solution is used. Clamond (2007) obtained a third-order Lagrangian solution for gravity waves in finite-depth water and a seventh-order solution for deep water waves; moreover, Henry (2009) studied the steady periodic flow induced by the Korteweg and de Vries equation. Longuet-Higgins (1986, 1987) and Chang *et al* (2009) found that the Lagrangian period of particle motion is different from the Eulerian wave period, with a higher Lagrangian mean level than the Eulerian mean level at the free surface in deep water.

From the above-mentioned discussions, it is clear that fewer experimental data are available to quantitatively demonstrate the characteristics of fluid particle behavior. One purpose of this study is to conduct an integrated experiment to investigate the Lagrangian properties, including particle orbit, Lagrangian mean level, Lagrangian wave frequency, mass transport velocity, wave profile, velocity distribution and wave pressure in progressive gravity water waves at uniform depth. Another goal is to establish a theory in which waves are irrotational and are perfectly constructed in the Lagrangian framework. A set of governing equations in Lagrangian coordinates is derived for two-dimensional progressive gravity waves in water at uniform depth. Expanding the unknown function in a small parameter expansion

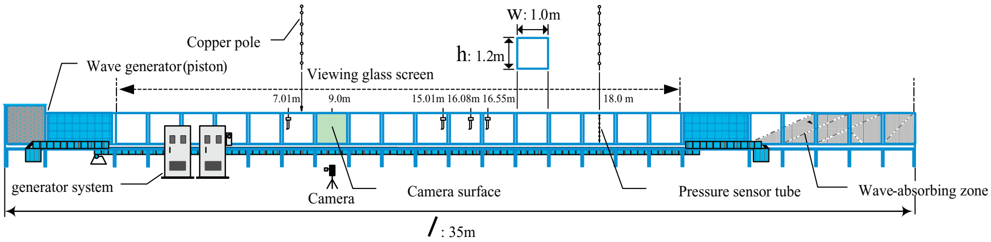

Figure 1. The experimental framework for this study.

related to the wave steepness, the Lagrangian wave frequency may be a function of the marked labels (a, b) of each individual particle, and the systematic asymptotic equations in Lagrangian variables may be deduced using the Lindstedt–Poincaré perturbation method. The fifth-order Lagrangian trajectory solution can thus be solved sequentially for each order of approximation. The Lagrangian wave period, the Lagrangian mean level and mass transport velocity up to fourth order are derived for all particles over the whole range of levels and are more general than the expression that is applicable only to the particles at the free surface (Longuet-Higgins 1986, 1987). Finally, to validate the accuracy of the analytical results, a series of laboratory experiments are performed. The Lagrangian properties of trajectories, the mass transport velocity, the Lagrangian mean wave level and wave pressure are shown to agree with experimental data very well.

2. Experimental process and definition of Lagrangian label

The aim of this experiment is to quantitatively investigate the characteristics of water particles for periodic progressive gravity waves at uniform water depth. The experimental processes are described below.

2.1. The experimental setup

To acquire the particle trajectory and wave pressure, a series of experimental measurements were carried out in a glass-walled wave tank, 35 m × 1.0 m × 1.2 m, in the Department of Marine Environment and Engineering, National Sun Yat-Sen University. A camera was set up in front of the glass wall at about 9.0 m to capture the particle motion. Eight pressure sensors were installed vertically equidistant from the still water surface to near-bottom on an erect column placed at 15 m from the end of the tank. Four wave gauges were located at 7.0, 15, 16 and 16.6 m from the wave generator to measure the incident waves. At the end of the tank, a 1:10 sloping rubberized-fiber wave-absorbing beach was built to prevent waves from reflecting. The beach was constructed so that, at the highest level examined, the longest-period waves would have to travel over three times their own wavelength over the beach material. Shorter-period waves were expected to be more readily absorbed by the beach than these long-period waves (Davies and Heathershaw 1984). The whole experimental framework is schematically shown in figure 1.

2.2. Measurement apparatus and procedure

1. Monochromatic waves were generated using a program-controlled electro-hydraulic piston-type wave generator. Wave period settings could be adjusted in increments of 0.01 s from the shortest generated wave period, 0.08 s, and independent checks of the

Figure 2. The transparent acrylic-plastic sheet was plotted with network grids in 2 cm × 2 cm intervals.

accuracy of these settings were carried out in the error range 0.2–0.5 s. by timing 50 oscillations of the wave generator bulkhead. The results of this investigation showed agreement to within $\pm$ 0.005 s of the nominal wave-period setting.

2. The incident progressive wave elevations and water pressures were measured by using Kenek CH-4-40-type wave gauges and Kyowa PGM-0.5GK-type pressure sensors, both of which have linear output.
3. Water particles were simulated with fluorescent spherical polystyrene (PS) beads with a diameter of about 0.1 cm. The density of primitive PS is about 1.05 g cm^{-3}, slightly heavier than water, but the PS density is approximately equal to a water density of 1.000 g cm^{-3} after boiling with water and will remain almost neutrally stable at a fixed position in water.
4. Images were captured by a high-speed camera (A301fc-type, Basler Company), which can take 80 frames per second. The camera was controlled by BCamGraber program and linked to a 1394 CARD to collect and analyze the data.
5. Four powerful lamps (110 V, 500 W) were set up to reinforce the brightness of the images of PS motion in the water waves for easier identification.
6. A transparent acrylic-plastic sheet (1 m × 45 cm × 2 mm) plotted with 2 cm × 2 cm square grids as shown in figure 2 was placed in the still water centered along the width of the tank. It was first photographed before being removed from the tank. The network grids in the photograph were programmed into the computer and used to analyze the continuous images of particle trajectories captured by the high-speed camera.
7. A copper pole (150 cm long with a diameter of 0.5 cm), calibrated at 0.1 cm intervals and perforated below 70 cm with 20 holes having a diameter of 0.3 cm, was erected vertically in front of the viewing glass in the still water tank. The PS was pushed out horizontally from the holes of the copper pole at different water levels into the still water. Then, the copper pole was slowly removed from the tank before the waves were generated to avoid interfering with the incident waves and PS motion.

2.3. Experimental results

The particle orbit experiments were conducted at four constant water depths d (50, 70, 80 and 90 cm) and various wave periods T_w (0.8–1.6 s). The wave height H after the generated progressive waves became stable (about seven waves) was varied over a range of about

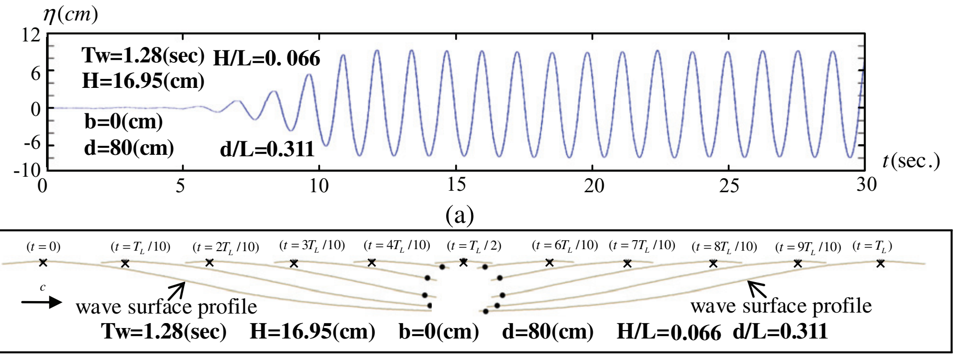

(b)

Figure 3. The typical records of the water surface elevation and the PS motion with larger experimental waves at the free surface: (a) is the water surface elevation, (b) is the positions of the PS motion at the same wave profile between two consecutive wave troughs and the symbols $\times$ and $\bullet$ denote, respectively, the wave crest and the PS position taken at the time interval $T_L/10$; T_L is the PS motion period.

3.7–17.0 cm. The particle motions were measured at different positions from the still water level to about a depth of 12 cm.

Typical water surface elevation and the particle motions at the free surface are shown in figures 3(a) and (b), respectively. Table 1 and figure 4 show all the measured results, and good quantitative consistency is found regarding the orbit, the particle motion period, the mass transport velocity and the Lagrangian mean level between the fifth-order theoretical results and experimental data. The wavelength used at relative water depth is calculated theoretically.

2.4. Definition of Lagrangian labels (a, b)

The fluid motion in the Lagrangian representation is described by tracing the individual fluid particles. For two-dimensional flow, fluid particles are distinguished by the horizontal and vertical parameters a, b, known as the Lagrangian labels. These labels have a one-to-one correlation with the initial particle positions (x_0, y_0), which has been demonstrated in, for example, section 16 by Lamb (1932) or by Yakubovich and Zenkovich (2001). The fluid motion is described by the set of particle trajectories $x(a, b, t)$ and $y(a, b, t)$, where x and y are, respectively, the horizontal and vertical Cartesian coordinates. The dependent variables x and y express the particle positions at time t and are functions of the independent variables a, b and t. It is still difficult to clearly define the Lagrangian labels (a, b).

The measurements of particle trajectories are shown in figure 4. The horizontal label a is generally marked along the horizontal x-axis, while the vertical label b is chosen to be in the original still water. In other words, it is equal to the wavelength-averaged $\bar{y}$ of the vertical displacement y of water particles along the direction of the wave propagation. Hence, from the conservation of mass and because the wave is periodic in time t and space x (or a)

$$
\begin{aligned}
\frac{1}{L}\int_x^{x+L}\int_{-d}^{\eta} \mathrm{d}y(a,b,t)\,\mathrm{d}x(a,b,t) &= \frac{1}{L}\int_x^{x+L}\int_{-d}^{\eta} \mathrm{d}y\,\mathrm{d}x \\
&= \frac{1}{L}\int_a^{a+L}\int_{-d}^{0} \frac{\partial(x,y)}{\partial(a,b)}\,\mathrm{d}b\,\mathrm{d}a = \frac{1}{L}\int_a^{a+L}\int_{-d}^{0} \mathrm{d}b\,\mathrm{d}a = d, \quad \text{i.e. } J = \frac{\partial(x,y)}{\partial(a,b)} = 1
\end{aligned}
\tag{1a}
$$

Table 1. Orbital experimental conditions and comparison of measured and theoretical results for the motion period T_L, mass transport velocity U_M and Lagrangian mean level $\bar{\eta}_L$ of the particle in the waves.

							T_L (s)		$U_M(0)$ (cm)		$\bar{\eta}_L$ (cm)	
No.	T_w(s)	d (cm)	H (cm)	b (cm)	H/L	d/L	Measured	Theory	Measured	Theory	Measured	Theory
1	1.000	50	3.77	0	0.025	0.329	1.007	1.006	0.96	0.95	0.11	0.08
2	1.000	50	4.78	0	0.031	0.327	1.011	1.010	1.57	1.53	0.13	0.12
3	0.790	50	4.94	0	0.050	0.503	0.820	0.810	3.09	3.07	0.21	0.20
4	1.090	50	5.02	0	0.028	0.283	1.102	1.099	1.40	1.37	0.13	0.12
5	1.060	50	5.30	0	0.031	0.296	1.073	1.071	1.67	1.63	0.14	0.14
6	0.820	50	9.10	0	0.082	0.449	0.880	0.877	8.86	8.81	0.62	0.61
7	1.090	50	9.80	0	0.054	0.277	1.127	1.125	5.18	5.13	0.48	0.46
8	1.010	50	10.58	0	0.066	0.312	1.059	1.057	7.11	7.04	0.60	0.59
9	1.390	50	11.56	0	0.044	0.192	1.426	1.424	4.51	4.45	0.51	0.49
10	1.020	50	13.95	0	0.083	0.299	1.101	1.098	11.59	11.52	1.01	0.99
11	1.330	50	14.56	0	0.059	0.202	1.389	1.387	7.62	7.51	0.82	0.81
12	0.800	70	4.80	0	0.047	0.686	0.820	0.818	2.81	2.78	0.22	0.18
13	1.000	70	5.00	0	0.032	0.447	1.011	1.010	1.63	1.59	0.14	0.13
14	1.210	70	5.60	0	0.025	0.316	1.218	1.218	1.23	1.20	0.13	0.12
15	1.410	70	5.69	0	0.020	0.246	1.417	1.416	0.89	0.88	0.10	0.10
16	1.000	70	7.26	0	0.046	0.442	1.024	1.021	3.34	3.31	0.28	0.27
17	1.000	70	8.90	0	0.056	0.438	1.034	1.032	4.95	4.91	0.41	0.40
18	1.500	70	9.79	0	0.031	0.222	1.518	1.517	2.31	2.29	0.29	0.27
19	0.790	80	4.81	0	0.048	0.802	0.811	0.809	2.92	2.89	0.20	0.19
20	0.790	80	4.84	0	0.049	0.802	0.812	0.809	2.95	2.93	0.20	0.19
21	0.790	80	4.85	0	0.049	0.802	0.811	0.809	3.03	2.94	0.20	0.19
22	1.010	80	5.25	0	0.033	0.499	1.022	1.021	1.72	1.69	0.14	0.14
23	1.000	80	5.30	0	0.034	0.508	1.012	1.011	1.81	1.77	0.13	0.14
24	1.200	80	5.70	0	0.026	0.361	1.212	1.208	1.27	1.23	0.13	0.12
25	1.250	80	5.80	0	0.024	0.336	1.259	1.258	1.19	1.15	0.13	0.12
26	1.490	80	5.80	0	0.018	0.251	1.495	1.495	0.81	0.76	0.10	0.09
27	1.060	80	10.40	0	0.058	0.444	1.098	1.096	5.67	5.60	0.50	0.49
28	1.280	80	10.90	0	0.043	0.318	1.307	1.305	3.81	3.78	0.41	0.39
29	1.000	80	11.20	0	0.069	0.491	1.051	1.049	7.61	7.54	0.64	0.63
30	1.210	80	12.40	0	0.054	0.348	1.251	1.247	5.62	5.58	0.54	0.55
31	1.560	80	12.50	0	0.036	0.231	1.585	1.583	3.24	3.22	0.41	0.40
32	1.280	80	16.95	0	0.066	0.311	1.343	1.340	8.92	8.89	0.95	0.94
33	1.020	90	11.30	0	0.067	0.531	1.069	1.067	7.30	7.24	0.60	0.61
34	1.220	90	12.35	0	0.053	0.383	1.258	1.255	5.36	5.32	0.52	0.53
35	1.220	90	16.30	0	0.068	0.376	1.282	1.279	9.11	9.05	0.91	0.92
36	1.170	50	6.98	−1.0	0.035	0.251	1.188	1.186	2.06	2.02	0.21	0.21
37	1.150	70	10.00	−2.0	0.049	0.340	1.179	1.178	3.84	3.77	0.39	0.40
38	1.000	50	5.10	−2.45	0.033	0.327	1.013	1.011	1.48	1.41	0.13	0.14
39	1.140	50	6.13	−4.0	0.032	0.262	1.156	1.153	1.45	1.41	0.14	0.17
40	1.350	70	15.70	−4.2	0.057	0.256	1.402	1.400	5.84	5.80	0.8	0.79
41	1.180	70	10.08	−5.5	0.047	0.325	1.209	1.207	2.96	2.92	0.40	0.39
42	0.970	70	8.40	−5.8	0.056	0.465	1.003	1.001	2.89	2.87	0.39	0.38
43	1.100	70	7.68	−6.0	0.041	0.371	1.121	1.119	1.91	1.89	0.29	0.25
44	1.300	70	9.70	−7.0	0.038	0.277	1.322	1.321	2.13	2.11	0.28	0.32
45	1.000	70	10.70	−11.1	0.066	0.433	1.045	1.045	2.84	2.81	0.60	0.58

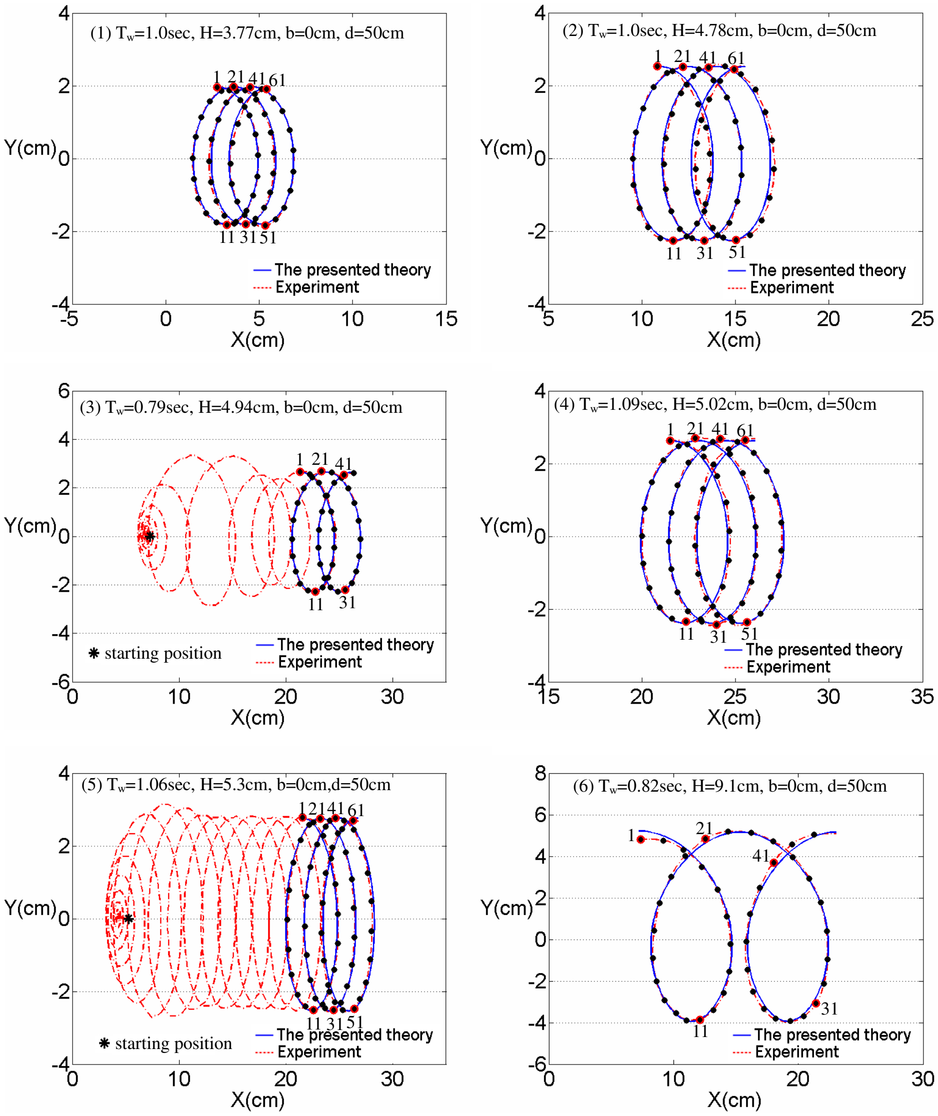

Figure 4. Comparison between the orbits of water particles obtained by the present theory and those obtained from experimental measurements of the PS motions at different water levels b for the various experimental wave cases. The symbol $*$ denotes the PS starting position in the still water; the first black point (•) marked with no. 1 is the PS position taken at the time when the wave crest just arrives; the time interval between two consecutive black point (•) PS positions is $T_w/20$, where T_w is the wave period.

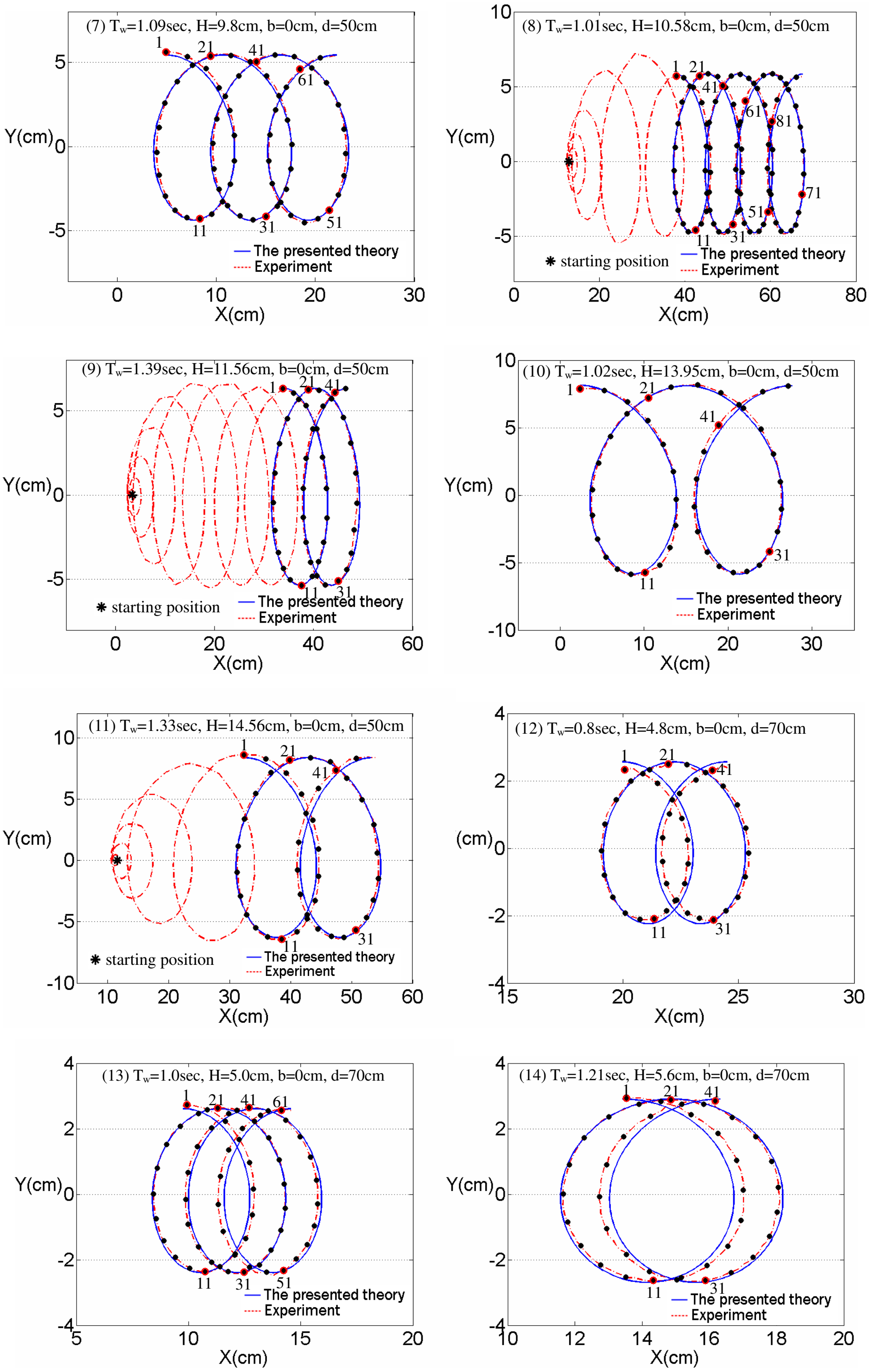

Figure 4. (Continued).

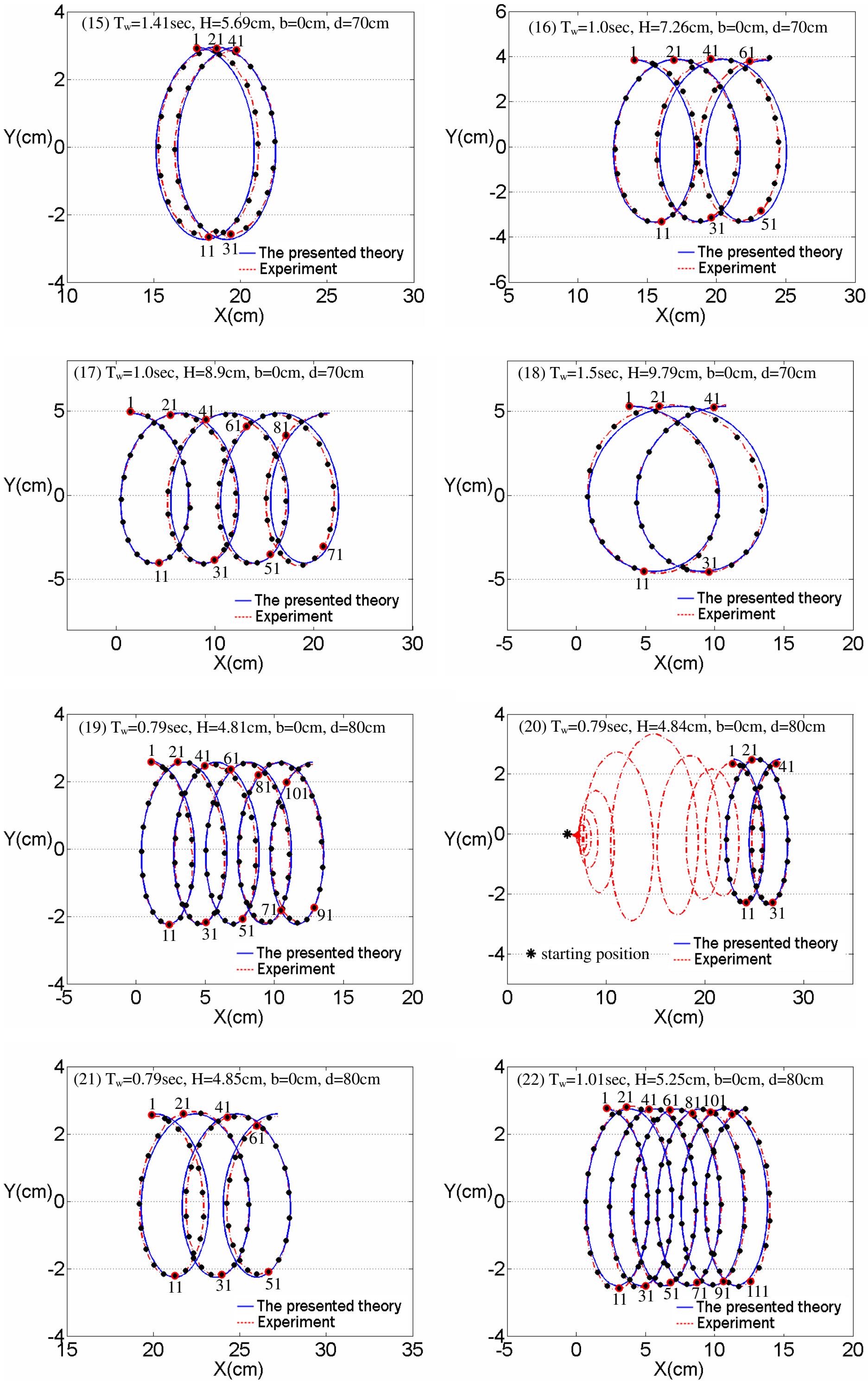

Figure 4. (Continued).

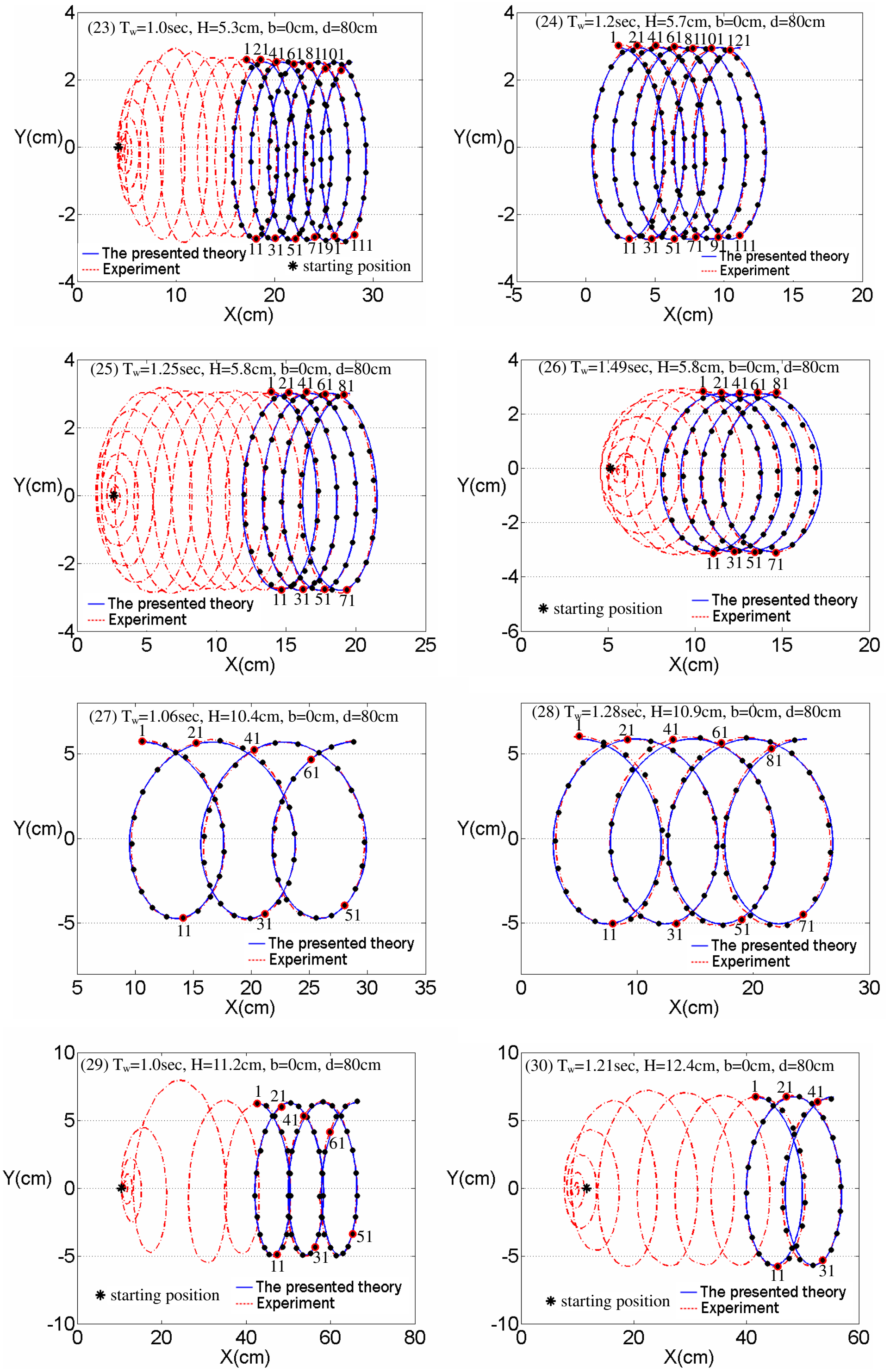

Figure 4. (Continued).

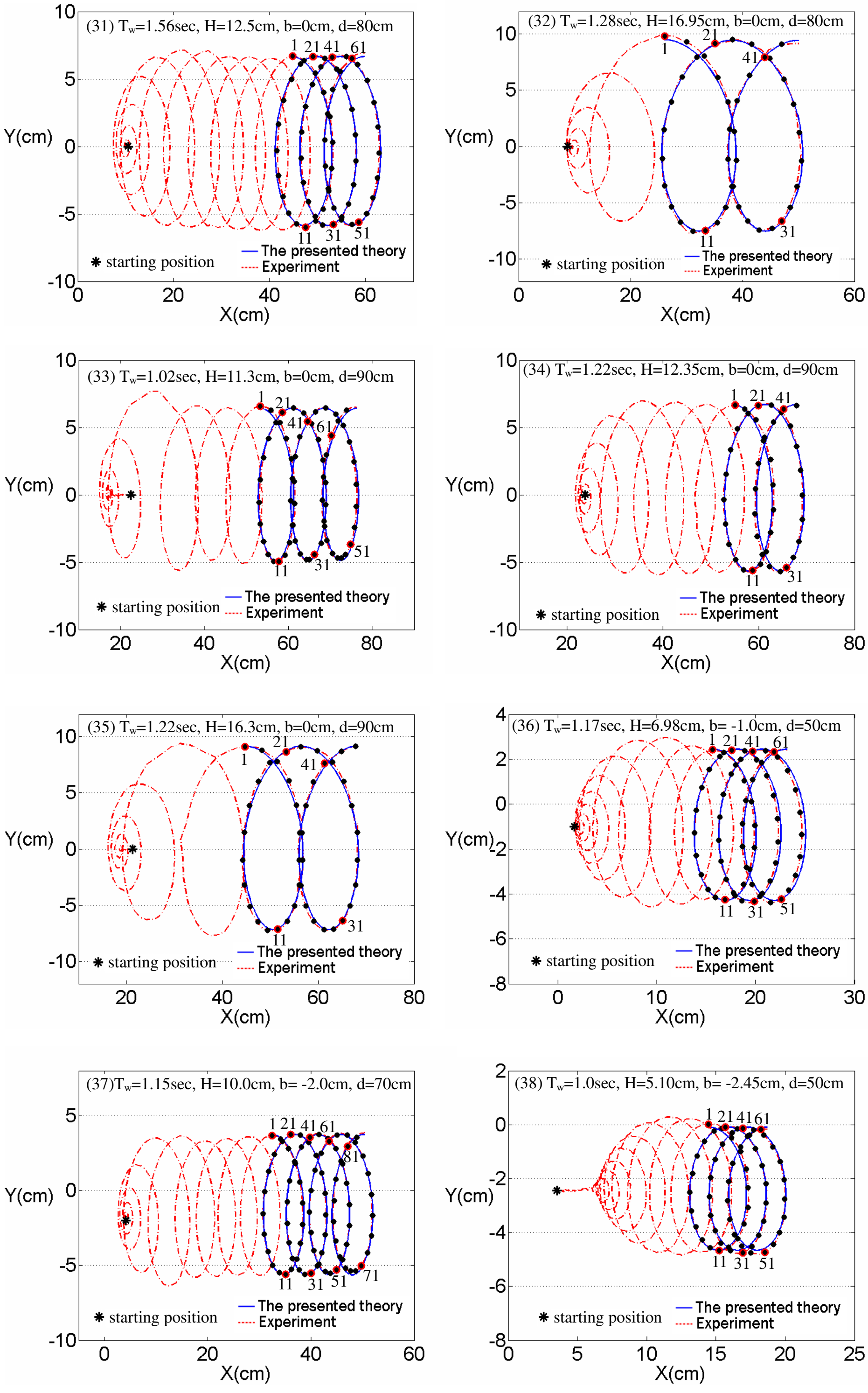

Figure 4. (Continued).

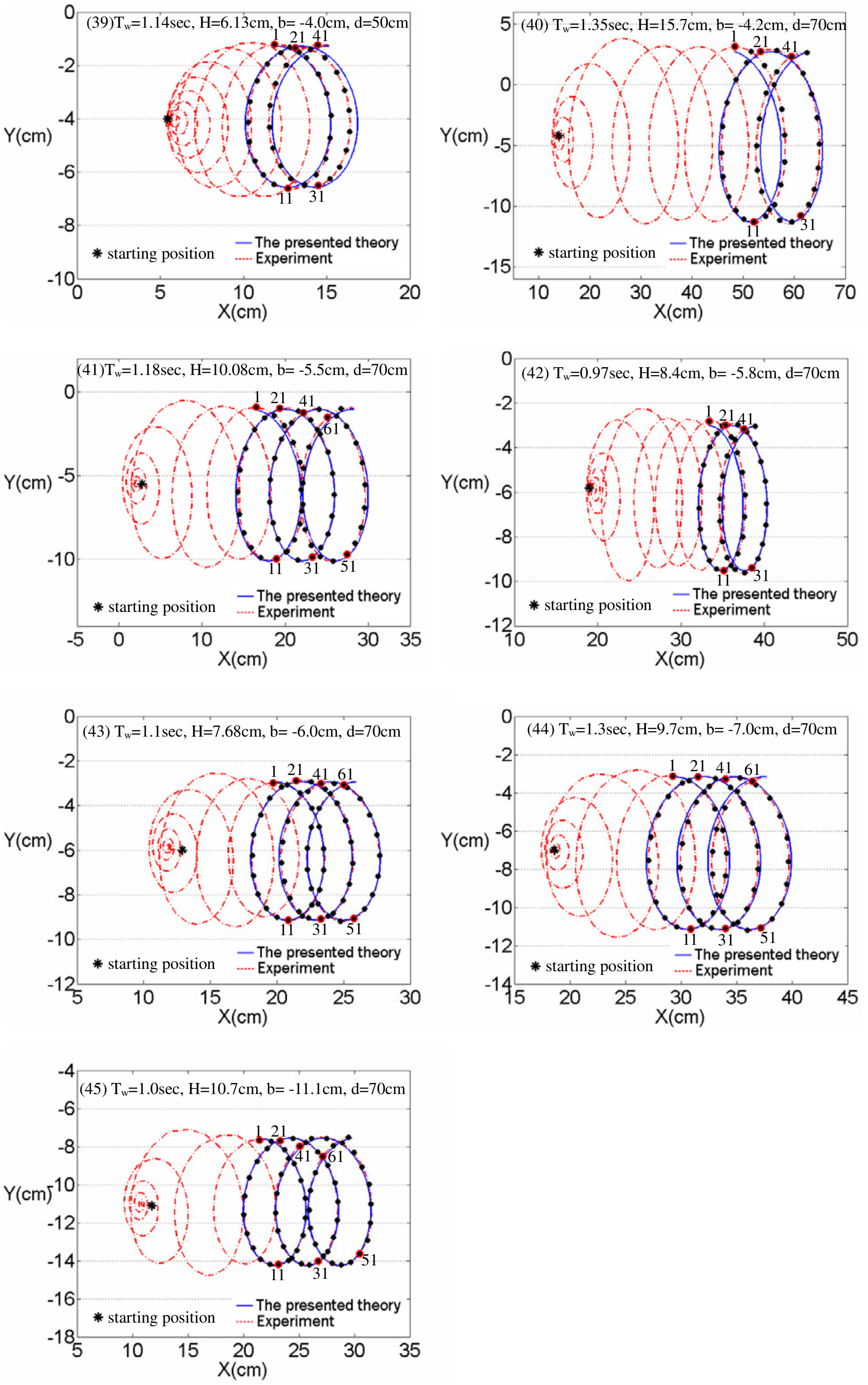

Figure 4. (Continued).

and the wavelength-averaged level $\bar{y}$ is

$$\bar{y} = \frac{1}{L}\int_{x(a,b,t)}^{x(a+L,b,t)} y(a,b,t)\,\mathrm{d}x(a,b,t) = \frac{1}{L}\int_{x}^{x+L}\int_{-d}^{y}\mathrm{d}y\,\mathrm{d}x - d$$
$$= \frac{1}{L}\int_{a}^{a+L}\int_{-d}^{b}\frac{\partial(x,y)}{\partial(a,b)}\mathrm{d}b\,\mathrm{d}a - d = b, \quad -d \leqslant b \leqslant 0, \tag{1b}$$

where $\eta = \eta(x(a,0,t))$ is the free surface profile and the wavelength-averaged η of the free surface profile is $(1/L)\int_0^L \eta\,\mathrm{d}x = 0$.

Based on the above physical definition of the Lagranigan labels (a, b) marked with the water particles in wave motion, a simple framework of the Lagrangian description is constructed. All the particles at the free surface with $b = 0$ and those at the bottom with $b = -d$ are defined in the Lagrangian labels (a, b) as is shown in equations (1*a*) and (1*b*).

3. Formulation of the problem and asymptotic solutions

Consider a two-dimensional monochromatic water wave that is propagating over a uniform horizontal impermeable bed. The positive horizontal x-axis is directed along the wave direction, while the y-axis is positive vertically upward from the still water level. d is the still water depth, $k = 2\pi/L$ is the wave number and $\sigma_{\mathrm{w}} = 2\pi/T_{\mathrm{w}}$ is the wave angular frequency, where L is the wavelength and T_{w} is the wave period.

The system of Lagrangian governing equations and boundary conditions for the two-dimensional irrotational free-surface flow is summarized below.

$$x_a y_b - x_b y_a = \frac{\partial(x,y)}{\partial(a,b)} = 1, \tag{2}$$

$$x_{at} y_b - x_{bt} y_a + x_a y_{bt} - x_b y_{at} = \frac{\partial(x_t,y)}{\partial(a,b)} + \frac{\partial(x,y_t)}{\partial(a,b)} = 0, \tag{3}$$

$$x_{at} x_b - x_{bt} x_a + y_{at} y_b - y_{bt} y_a = \frac{\partial(x_t,x)}{\partial(a,b)} + \frac{\partial(y_t,y)}{\partial(a,b)} = 0, \tag{4}$$

$$\frac{\partial\phi}{\partial a} = x_t x_a + y_t y_a, \quad \frac{\partial\phi}{\partial b} = x_t x_b + y_t y_b, \tag{5}$$

$$\frac{p}{\rho} = -\frac{\partial\phi}{\partial t} - gy + \frac{1}{2}(x_t^2 + y_t^2), \tag{6}$$

$$p = 0, \quad b = 0, \tag{7}$$

$$v = y_t = 0, \quad y = b = -d. \tag{8}$$

In equations (2)–(8), the subscripts a, b and t denote partial differentiation with respect to the specified variable, $p(a,b,t)$ is the water pressure, $\phi(a,b,t)$ is the velocity potential function in the Lagrangian system and g is the gravitational acceleration. Except for equations (5) and (6), the fundamental physical relationships that define the above equations have been derived by many authors (Miche 1944, Lamb 1932, Yakubovich and Zenkovich 2001, Mei 1983). Equation (2) is the continuity equation and equation (3) is the differentiation of equation (2) with respect to time t. Equations (4) and (5) denote the irrotational flow condition and the corresponding Lagrangian velocity potential, respectively. Equation (6) is the Weber transform for the irrotational flow in the Lagrangian description, which is demonstrated in appendix A along with equations (4) and (5). Equation (7) represents the dynamic boundary condition of zero pressure at the free surface. Equation (8) is the bottom boundary condition of zero vertical velocity.

To solve the nonlinear equations (2)–(8), we introduce the Lagrangian angular frequency σ of particle motion and use the perturbation method. In the Lagrangian approach, the particle positions x and y, the potential function ϕ and pressure p are considered to be functions of independent variables a and b and time t. These solutions are sought in perturbation series by introducing an ordering symbol ϵ, which is inserted to identify the order of the associated term (Pierson 1962, Chen 1994a, 1994b, Piedra-Cueva 1995)

$$x = x(a, b, t) = a + \sum_{n=1}^{\infty} \varepsilon^n [f_n(a, b, \sigma t) + f_n'(a, b, \sigma_0 t)], \tag{9}$$

$$y = y(a, b, t) = b + \sum_{n=1}^{\infty} \varepsilon^n [g_n(a, b, \sigma t) + g_n'(a, b, \sigma_0 t)], \tag{10}$$

$$\phi = \phi(a, b, t) = \sum_{n=1}^{\infty} \varepsilon^n [\phi_n(a, b, \sigma t) + \phi_n'(a, b, \sigma_0 t)], \tag{11}$$

$$p = p(a, b, t) = -\rho g b + \sum_{n=1}^{\infty} \varepsilon^n p_n(a, b, \sigma t), \tag{12}$$

$$\sigma = \sigma(a, b) = \sigma_0 + \sum_{n=1}^{\infty} \varepsilon^n \sigma_n(a, b) = 2\pi / T_{\mathrm{L}}(a, b), \tag{13}$$

where the Lagrangian variables (a, b) are defined in section 2.4 as the two characteristic parameters. In these expressions, f_n, g_n, ϕ_n and p_n are expected to be associated with nth-order harmonic solutions. f_n', g_n' and ϕ_n' are non-periodic functions, $\sigma = 2\pi/T_{\mathrm{L}}$ is the particle motion angular frequency, or the Lagrangian angular frequency for a particle reappearing at its highest or lowest elevation. T_{L} is the corresponding particle motion period. Substituting equations (9)–(13) into (2)–(8), and collecting terms of equal ϵ order, we obtain a sequence of non-homogeneous governing equations that can be solved, as shown in the following sections.

3.1. First-order approximation

Collecting terms of order ϵ, the governing equations and the boundary conditions are

$$f_{1a} + f_{1a}' + g_{1b} + g_{1b}' = 0, \tag{14a}$$

$$\sigma_0 (f_{1a\sigma t} + f_{1a\sigma_0 t}' + g_{1b\sigma t} + g_{1b\sigma_0 t}') = 0, \tag{14b}$$

$$\sigma_0 (f_{1b\sigma t} + f_{1b\sigma_0 t}' - g_{1a\sigma t} - g_{1a\sigma_0 t}') = 0, \tag{14c}$$

$$\phi_{1a} + \phi_{1a}' = \sigma_0 (f_{1\sigma t} + f_{1\sigma_0 t}'), \tag{14d}$$

$$\phi_{1b} + \phi_{1b}' = \sigma_0 (g_{1\sigma t} + g_{1\sigma_0 t}'), \tag{14e}$$

$$\frac{p_1}{\rho} = -\sigma_0 (\phi_{1\sigma t} + \phi_{1\sigma_0 t}') - g(g_1 + g_1'), \tag{14f}$$

$$p_1 = 0, \quad b = 0, \tag{14g}$$

$$g_{1\sigma t} = g_{1\sigma_0 t}' = 0, \quad b = -d. \tag{14h}$$

The flow is assumed to be periodic with a crest at $a = 0$ and $t = 0$, such that the first-order solution is easily written as

$$f_1' = g_1' = \phi_1' = 0, \quad \sigma_0^2 = gk \tanh kd = gkT, \quad T = \tanh kd, \tag{15}$$

$$f_1 = -\alpha \frac{\cosh k(b+d)}{\cosh kd} \sin(ka - \sigma t), \tag{16}$$

$$g_1 = \alpha \frac{\sinh k(b+d)}{\cosh kd} \cos(ka - \sigma t), \tag{17}$$

$$\phi_1 = \frac{\alpha\sigma_0}{k} \frac{\cosh k(b+d)}{\cosh kd} \sin(ka - \sigma t), \tag{18}$$

$$\frac{p_1}{\rho} = -\alpha g \frac{\sinh kb}{\cosh^2 kd} \cos(ka - \sigma t), \tag{19}$$

where the parameter α represents the amplitude function of the particle displacement; the wave amplitude is usually taken as $a_0 = \alpha \tanh kd$. $\phi_1(a, b, t)$ is the first-order Lagrangian velocity potential, and $p_1(a, b, t)$ is the first-order wave dynamic pressure in the Lagrangian form with pressure $p_1 = 0$ at the free surface $b = 0$. Equations (15)–(19) satisfy all the first-order hydrodynamic equations (14*a*)–(14*h*) formulated in Lagrangian terms including the irrotational condition, which differ from Gerstner's wave at infinite water depth that possesses finite vorticity and even becomes infinite at the free surface in the limiting Gerstner's wave (Constantin 2001a, Constantin *et al* 2007, Henry 2008). The linear dispersion relation shows that the first-order Lagrangian angular frequency σ_0 of particle motion is the same as the first-order Stokes wave angular frequency in the Eulerian approach. The first-order free surface in Lagrangian coordinates is given by setting $b = 0$ in equations (16) and (17) and is similar to the expression for the profile found from the first-order Eulerian equations.

3.2. Second-order approximation

After substituting the first-order solution, the second-order governing equations in terms of ϵ^2, including the continuity equation and the irrotational condition, are given by

$$\begin{aligned} f_{2a} + f_{2a}' + g_{2b} + g_{2b}' &= f_{1b}g_{1a} - f_{1a}g_{1b} - (\sigma_{1a} f_{1\sigma t} + \sigma_{1b} g_{1\sigma t})t \\ &= \frac{1}{2}\alpha^2 k^2 \left[\frac{\cosh 2k(b+d)}{\cosh^2 kd} + \frac{\cos 2(ka - \sigma t)}{\cosh^2 kd} \right] \\ &\quad - \alpha \left[\sigma_{1a} \frac{\cosh k(b+d)}{\cosh kd} \cos(ka - \sigma t) + \sigma_{1b} \frac{\sinh k(b+d)}{\cosh kd} \sin(ka - \sigma t) \right] t, \end{aligned} \tag{20}$$

$$\begin{aligned} &\sigma_0(f_{2a\sigma t} + f_{2a\sigma_0 t}' + g_{2b\sigma t} + g_{2b\sigma_0 t}') \\ &\quad = \sigma_0(f_{1b}g_{1a} - f_{1a}g_{1b})_{\sigma t} - \sigma_1(f_{1a} + g_{1b})_{\sigma t} - \sigma_{1a} f_{1\sigma t} - \sigma_{1b} g_{1\sigma t} \\ &\qquad - \sigma_0[\sigma_{1a} f_{1(\sigma t)^2} + \sigma_{1b} g_{1(\sigma t)^2}]t \\ &\quad = \alpha^2 k^2 \sigma_0 \frac{\sin 2(ka - \sigma t)}{\cosh^2 kd} - \alpha\sigma_{1a} \frac{\cosh k(b+d)}{\cosh kd} [\cos(ka - \sigma t) \\ &\qquad + \sigma_0 t \sin(ka - \sigma t)] - \alpha\sigma_{1b} \frac{\sinh k(b+d)}{\cosh kd} [\sin(ka - \sigma t) - \sigma_0 t \cos(ka - \sigma t)], \end{aligned} \tag{21}$$

$$
\begin{aligned}
&\sigma_0(f_{2b\sigma t}+f'_{2b\sigma_0 t}-g_{2a\sigma t}-g'_{2a\sigma_0 t})\\
&\qquad=\sigma_0(f_{1a\sigma t}f_{1b}-f_{1a}f_{1b\sigma t}+g_{1a\sigma t}g_{1b}-g_{1a}g_{1b\sigma t})+\sigma_1(g_{1a}-f_{1b})_{\sigma t}\\
&\qquad\quad+\sigma_{1a}g_{1\sigma t}-\sigma_{1b}f_{1\sigma t}+\sigma_0[\sigma_{1a}g_{1(\sigma t)^2}-\sigma_{1b}f_{1(\sigma t)^2}]t\\
&\qquad=\alpha^2k^2\sigma_0\frac{\sinh 2k(b+d)}{\cosh^2 kd}+\alpha\sigma_{1a}\frac{\sinh k(b+d)}{\cosh kd}[\sin(ka-\sigma t)-\sigma_0 t\cos(ka-\sigma t)]\\
&\qquad\quad-\alpha\sigma_{1b}\frac{\cosh k(b+d)}{\cosh kd}[\cos(ka-\sigma t)+\sigma_0 t\sin(ka-\sigma t)],
\end{aligned}
\tag{22}
$$

For gravity waves of permanent form, the terms $t\cos(ka-\sigma t)$ and $t\sin(ka-\sigma t)$ that increase linearly with time have to be zero to avoid resonance. We have $\sigma_{1a}=\sigma_{1b}=0$ and $\sigma_1=w_1=$ constant. Then the general solution that satisfies the bottom boundary condition can be written as

$$
\begin{aligned}
f_2&=-\beta_2\frac{\cosh 2k(b+d)}{\cosh^2 kd}\sin 2(ka-\sigma t)+\frac{1}{4}\alpha^2k\frac{\sin 2(ka-\sigma t)}{\cosh^2 kd}-\lambda_2\frac{\cosh k(b+d)}{\cosh kd}\sin(ka-\sigma t),\\
f'_2&=\frac{1}{2}\alpha^2k\frac{\cosh 2k(b+d)}{\cosh^2 kd}\sigma_0 t,\\
g_2&=\beta_2\frac{\sinh 2k(b+d)}{\cosh^2 kd}\cos 2(ka-\sigma t)+\lambda_2\frac{\sinh k(b+d)}{\cosh kd}\cos(ka-\sigma t),\\
g'_2&=\frac{1}{4}\alpha^2k\frac{\sinh 2k(b+d)}{\cosh^2 kd}.
\end{aligned}
\tag{23}
$$

Inserting equation (23) into (5) in ϵ^2 order, we deduce

$$
\begin{aligned}
\phi_{2a}&=\sigma_0(f_{2\sigma t}+f'_{2\sigma_0 t})+\sigma_0(f_{1a}f_{1\sigma t}+g_{1a}g_{1\sigma t})+\sigma_1 f_{1\sigma t}-\sigma_{1a}t\phi_{1\sigma t}-\phi'_{2a}\\
&=\sigma_0\left[2\beta_2\frac{\cosh 2k(b+d)}{\cosh^2 kd}\cos 2(ka-\sigma t)-\alpha^2k\frac{\cos 2(ka-\sigma t)}{\cosh^2 kd}\right]\\
&\quad+(\alpha w_1+\sigma_0\lambda_2)\frac{\cosh k(b+d)}{\cosh kd}\cos(ka-\sigma t)-\phi'_{2a},
\end{aligned}
$$

$$
\begin{aligned}
\phi_{2b}&=\sigma_0(g_{2\sigma t}+g'_{2\sigma_0 t})+\sigma_0(f_{1b}f_{1\sigma t}+g_{1b}g_{1\sigma t})+\sigma_1 g_{1\sigma t}-\sigma_{1b}t\phi_{1\sigma t}-\phi'_{2b}\\
&=2\sigma_0\beta_2\frac{\sinh 2k(b+d)}{\cosh^2 kd}\sin 2(ka-\sigma t)\\
&\quad+(\alpha w_1+\sigma_0\lambda_2)\frac{\sinh k(b+d)}{\cosh kd}\sin(ka-\sigma t)-\phi'_{2b},
\end{aligned}
\tag{24}
$$

Note that the secular terms in equation (24) have to be omitted, which yields $\alpha w_1+\sigma_0\lambda_2=0$. The second-order Lagrangian velocity potential is obtained by integrating over the Lagrangian variables a or b:

$$
\begin{aligned}
\phi_2&=\frac{\sigma_0}{k}\beta_2\frac{\cosh 2k(b+d)}{\cosh^2 kd}\sin 2(ka-\sigma t)-\frac{1}{2}\alpha^2\sigma_0\frac{\sin 2(ka-\sigma t)}{\cosh^2 kd},\\
\phi'_2&=D'_2(\sigma_0 t).
\end{aligned}
\tag{25}
$$

Substituting the solutions up to the second order into equation (5) in ϵ^2 order and applying the zero pressure condition at the free surface, the unknown coefficients are obtained as

$$\frac{p_2}{\rho} = -\sigma_0(\phi_{2\sigma t} + \phi'_{2\sigma_0 t}) - g(g_2 + g'_2) + \frac{1}{2}\sigma_0^2(f_{1\sigma t}^2 + g_{1\sigma t}^2) - \sigma_1\phi_{1\sigma t}$$
$$= g\left\{\beta_2\left[2\frac{\cosh 2k(b+d)}{\cosh^2 kd}T - \frac{\sinh 2k(b+d)}{\cosh^2 kd}\right] - \frac{3}{4}\alpha^2 kT(1-T^2)\right\}$$
$$\times \cos 2(ka - \sigma t) + \left[\alpha\frac{\sigma_0}{k}w_1\frac{\cosh k(b+d)}{\cosh kd} - g\lambda_2\frac{\sinh k(b+d)}{\cosh kd}\right]\cos(ka-\sigma t)$$
$$+ \frac{1}{4}\alpha^2\sigma_0^2\left[\frac{\cosh 2k(b+d)}{\cosh^2 kd} - \frac{\sinh 2k(b+d)}{T\cosh^2 kd}\right] - \sigma_0 D'_{2\sigma_0 t}, \tag{26}$$

$$w_1 = \lambda_2 = 0, \quad \beta_2 = \tfrac{3}{8}\alpha^2 k(\tanh^{-2} kd - 1),$$
$$\phi'_2 = D'_2(\sigma_0 t) = \tfrac{1}{4}\alpha^2\sigma_0^2(\tanh^2 kd - 1)t.$$

The second-order Lagrangian solutions are assembled as

$$f_2 = \alpha^2 k\left[-\frac{3}{8}(T^{-2} - T^2)\frac{\cosh 2k(b+d)}{\cosh 2kd} + \frac{1}{4}(1-T^2)\right]\sin 2(ka - \sigma t), \tag{27}$$

$$f'_2 = \frac{1}{2}\alpha^2 k(1+T^2)\frac{\cosh 2k(b+d)}{\cosh 2kd}\sigma_0 t, \tag{28}$$

$$g_2 = \frac{3}{8}\alpha^2 k(T^{-2} - T^2)\frac{\sinh 2k(b+d)}{\cosh 2kd}\ \cos 2(ka - \sigma t), \tag{29}$$

$$g'_2 = \frac{1}{4}\alpha^2 k(1+T^2)\frac{\sinh 2k(b+d)}{\cosh 2kd}, \tag{30}$$

$$\phi_2 = \alpha^2\sigma_0\left[\frac{3}{8}(T^{-2} - T^2)\frac{\cosh 2k(b+d)}{\cosh 2kd} - \frac{1}{2}(1-T^2)\right]\sin 2(ka - \sigma t),$$
$$\phi'_2 = -\tfrac{1}{4}\alpha^2\sigma_0^2(1-T^2)t, \quad \sigma_1 = 0, \tag{31}$$

$$\frac{p_2}{\rho} = g\alpha^2 k\left\{\frac{3}{8}(T^{-2} - 1)\left[2(T+T^3)\frac{\cosh 2k(b+d)}{\cosh 2kd}\right.\right.$$
$$\left.\left. -(1+T^2)\frac{\sinh 2k(b+d)}{\cosh 2kd}\right] - \frac{3}{4}(T - T^3)\right\}\cos 2(ka - \sigma t)$$
$$+\frac{1}{4}g\alpha^2 k\left\{\left[(T+T^3)\frac{\cosh 2k(b+d)}{\cosh 2kd} - (1+T^2)\frac{\sinh 2k(b+d)}{\cosh 2kd}\right] - (T^3 - T)\right\}. \tag{32}$$

The horizontal particle trajectory x in the second-order approximation includes a periodic component f_2 and a non-periodic function f'_2, which represents the second-order classical Stokes mass transport increasing linearly with time but decreasing exponentially with the depth b of the particle. This implies that a fluid particle moves forward and does not form a closed orbit, as in the first-order approximation. The vertical trajectory y in this order includes a second harmonic component g_2 and a term g'_2 that is a function of b only and is independent of time. This second-order vertical mean particle level g_2' exponentially decays with the depth b of the particle. Equation (30) also confirms that the Lagrangian mean level is higher than the Eulerian mean level (Longuet-Higgins 1986). Unlike Longuet-Higgins (1986, 1987) and Chang *et al* (2009) who used the Euler–Lagrange transformation to derive this result, the theory presented here is perfectly constructed in the Lagrangian framework for all particles from the free surface to the bottom.

3.3. Third- to fifth-order approximations

The third-order governing equations and boundary conditions can be obtained by substituting the first- and second-order approximations into equations (2)–(8) and then taking the terms of $O(\epsilon^3)$:

$$\begin{aligned}
f_{3a}+f_{3a}'+g_{3b}+g_{3b}' &= f_{1b}g_{2a}+(f_{2b}+f_{2b}')g_{1a}-f_{1a}(g_{2b}+g_{2b}')-f_{2a}g_{1b}\\
&\quad -(\sigma_{2a}f_{1\sigma t}+\sigma_{2b}g_{1\sigma t})t,\\
&=\alpha k^2\left(2\beta_2+\frac{1}{4}\alpha^2 k\right)\frac{\cosh 3k(b+d)}{\cosh^3 kd}\cos(ka-\sigma t)\\
&\quad +\alpha k^2\left(2\beta_2-\frac{1}{4}\alpha^2 k\right)\frac{\cosh k(b+d)}{\cosh^3 kd}\cos 3(ka-\sigma t)\\
&\quad -\alpha\left\{\sigma_{2a}\frac{\cosh k(b+d)}{\cosh kd}\cos(ka-\sigma t)\right.\\
&\quad \left.+\left[\alpha^2 k^3\sigma_0\frac{\sinh 2k(b+d)}{\cosh^2 kd}+\sigma_{2b}\right]\frac{\sinh k(b+d)}{\cosh kd}\sin(ka-\sigma t)\right\}t
\end{aligned}\tag{33}$$

$$\begin{aligned}
\sigma_0(f_{3a\sigma t}+f_{3a\sigma_0 t}'+g_{3b\sigma t}+g_{3b\sigma_0 t}') &= -\sigma_2(f_{1a}+g_{1b})_{\sigma t}-\sigma_{2a}f_{1\sigma t}-\sigma_{2b}g_{1\sigma t}\\
&\quad -\sigma_0[\sigma_{2a}f_{1(\sigma t)^2}+\sigma_{2b}g_{1(\sigma t)^2}]t+\sigma_0[(f_{1b}g_{2a}-f_{2a}g_{1b})_{\sigma t}+(f_{2b\sigma t}+f_{2b\sigma_0 t}')g_{1a}\\
&\quad +(f_{2b}+f_{2b}')g_{1a\sigma t}-f_{1a\sigma t}(g_{2b}+g_{2b}')-f_{1a}g_{2b\sigma t}]t.\\
&=\alpha k^2\sigma_0\left[\left(2\beta_2+\frac{1}{4}\alpha^2 k\right)\frac{\cosh 3k(b+d)}{\cosh^3 kd}\sin(ka-\sigma t)\right.\\
&\quad \left.+\left(6\beta_2-\frac{3}{4}\alpha^2 k\right)\frac{\cosh k(b+d)}{\cosh^3 kd}\sin 3(ka-\sigma t)\right]\\
&\quad -\alpha\left\{\sigma_{2a}\frac{\cosh k(b+d)}{\cosh kd}\cos(ka-\sigma t)+\left[\alpha^2 k^3\sigma_0\frac{\sinh 2k(b+d)}{\cosh^2 kd}+\sigma_{2b}\right]\right.\\
&\quad \left.\times\frac{\sinh k(b+d)}{\cosh kd}\sin(ka-\sigma t)\right\}\\
&\quad -\alpha\sigma_0\left\{\sigma_{2a}\frac{\cosh k(b+d)}{\cosh kd}\sin(ka-\sigma t)-\left[\alpha^2 k^3\sigma_0\frac{\sinh 2k(b+d)}{\cosh^2 kd}+\sigma_{2b}\right]\right.\\
&\quad \left.\times\frac{\sinh k(b+d)}{\cosh kd}\cos(ka-\sigma t)\right\}t,
\end{aligned}\tag{34}$$

$$\begin{aligned}
&\sigma_0(f_{3b\sigma t}+f'_{3b\sigma_0 t}-g_{3a\sigma t}-g'_{3a\sigma_0 t})\\
&\quad=\sigma_0[f_{2a\sigma t}f_{1b}-f_{2a}f_{1b\sigma t}+f_{1a\sigma t}(f_{2b}+f'_{2b})-f_{1a}(f_{2b\sigma t}+f'_{2b\sigma_0 t})\\
&\qquad+g_{2a\sigma t}g_{1b}-g_{2a}g_{1b\sigma t}+g_{1a\sigma t}(g_{2b}+g'_{2b})-g_{1a}g_{2b\sigma t}]-\sigma_2(f_{1b}-g_{1a})_{\sigma t}\\
&\qquad+\sigma_{2a}g_{1\sigma t}-\sigma_{2b}f_{1\sigma t}+\sigma_0[\sigma_{2a}g_{1(\sigma t)^2}-\sigma_{2b}f_{1(\sigma t)^2}]t\\
&\quad=\alpha k^2\sigma_0\left[(6\beta_2+\frac{3}{4}\alpha^2 k)\frac{\sinh 3k(b+d)}{\cosh^3 kd}\cos(ka-\sigma t)+\left(2\beta_2+\frac{1}{4}\alpha^2 k\right)\right.\\
&\qquad\left.\times\frac{\sinh k(b+d)}{\cosh^3 kd}\cos 3(ka-\sigma t)\right]\\
&\qquad+a\left\{\sigma_{2a}\frac{\sinh k(b+d)}{\cosh kd}\sin(ka-\sigma t)-\left[\frac{1}{2}\alpha^2k^3\sigma_0\frac{\sinh k(b+d)}{\cosh^3 kd}\right.\right.\\
&\qquad\left.\left.+\sigma_{2b}\frac{\cosh k(b+d)}{\cosh kd}\right]\cos(ka-\sigma t)\right\}\\
&\qquad-\alpha\sigma_0\left\{\sigma_{2a}\frac{\sinh k(b+d)}{\cosh kd}\cos(ka-\sigma t)+\left[\alpha^2k^3\sigma_0\frac{\sinh 2k(b+d)}{\cosh^2 kd}+\sigma_{2b}\right]\right.\\
&\qquad\left.\times\frac{\cosh k(b+d)}{\cosh kd}\sin(ka-\sigma t)\right\}t,
\end{aligned}\tag{35}$$

$$\begin{aligned}
\phi_{3a}+\phi'_{3a}&=\sigma_0[f_{3\sigma t}+f'_{3\sigma_0 t}+(f_{2\sigma t}+f'_{2\sigma_0 t})f_{1a}+f_{1\sigma t}f_{2a}+g_{2\sigma t}g_{1a}+g_{1\sigma t}g_{2a}]\\
&\quad+\sigma_2 f_{1\sigma t}-\sigma_{2a}t\phi_{1\sigma t},
\end{aligned}\tag{36a}$$

$$\begin{aligned}
\phi_{3b}+\phi'_{3b}&=\sigma_0[g_{3\sigma t}+g'_{3\sigma_0 t}+(f_{2\sigma t}+f'_{2\sigma_0 t})f_{1b}+(f_{2b}+f'_{2b})f_{1\sigma t}+g_{2\sigma t}g_{1b}\\
&\quad+(g_{2b}+g'_{2b})g_{1\sigma t}]+\sigma_2 g_{1\sigma t}-\sigma_{2b}t\phi_{1\sigma t},
\end{aligned}\tag{36b}$$

$$\frac{p_3}{\rho}=-[\sigma_0(\phi_{3\sigma t}+\phi'_{3\sigma_0 t})+g(g_3+g'_3)]+\sigma_0^2[(f_{2\sigma t}+f'_{2\sigma_0 t})f_{1\sigma t}+g_{2\sigma t}g_{1\sigma t}]-\sigma_2\phi_{1\sigma t}.\tag{37}$$

$$p_3=0,\quad b=0,\tag{38}$$

$$g_{3\sigma t}=g'_{3\sigma_0 t}=0,\quad b=-d.\tag{39}$$

The procedure to obtain the solutions at this order is similar to that of $O(\epsilon^2)$. It is noted that from equations (33)–(36b) it is possible to obtain $\sigma_{2a}=0$, $\sigma_{2b}t=-\alpha^2k^3\sigma_0 t \times \sinh 2k(b+d)/\cosh^2 kd=-kf'_{2b}$. After a lengthy but straightforward manipulation, the third-order Lagrangian solutions are given by

$$\sigma_2=\frac{1}{16}\alpha^2k^2\sigma_0(9T^{-2}-10+9T^2)-\frac{1}{2}\alpha^2k^2\sigma_0(1+T^2)\frac{\cosh 2k(b+d)}{\cosh 2kd}=\sigma_{w2}-k\frac{\partial f'_2}{\partial t},\tag{40}$$

$$f_3 = \alpha^3 k^2[\beta_{333} \sin 3(ka - \sigma t) + \beta_{331}\ \sin(ka - \sigma t)]\frac{\cosh 3k(b+d)}{\cosh 3kd}$$
$$+\alpha^3 k^2[\beta_{313} \sin 3(ka - \sigma t) + \beta_{311}\ \sin(ka - \sigma t)]\frac{\cosh k(b+d)}{\cosh kd}, \quad f_3' = 0, \tag{41}$$

$$g_3 = \alpha^3 k^2[\lambda_{333} \cos 3(ka - \sigma t) + \lambda_{331} \cos(ka - \sigma t)]\frac{\sinh 3k(b+d)}{\cosh 3kd}$$
$$+\alpha^3 k^2[\lambda_{313} \cos 3(ka - \sigma t) + \lambda_{311} \cos(ka - \sigma t)]\frac{\sinh k(b+d)}{\cosh kd}, \quad g_3' = 0, \tag{42}$$

$$\phi_3 = \alpha^3 k\sigma_0 \left\{ \left[\lambda_{333}\frac{\cosh 3k(b+d)}{\cosh 3kd} - \frac{1}{16}(9T^{-2} - 22 + 13T^2)\frac{\cosh k(b+d)}{\cosh kd} \right] \sin 3(ka - \sigma t) \right.$$
$$\left. + \frac{1}{16}(3T^{-2} + 6 - 9T^2)\frac{\cosh 3k(b+d)}{\cosh 3kd} \sin(ka - \sigma t) \right\}, \quad \phi_3' = 0, \tag{43}$$

$$\frac{p_3}{\rho} = g\alpha^3 k^2 \left\{ \frac{1}{64}(9T^{-4} - 22T^{-2} + 13) \right.$$
$$\times \left[(3T + 9T^3)\frac{\cosh 3k(b+d)}{\cosh 3kd} - (1 + 3T^2)\frac{\sinh 3k(b+d)}{\cosh 3kd} \right]$$
$$-\frac{1}{16}(21T^{-1} - 50T + 29T^3)\frac{\cosh k(b+d)}{\cosh kd}$$
$$\left. +\frac{1}{16}(3T^{-2} - 6 + 3T^2)\frac{\sinh k(b+d)}{\cosh kd} \right\} \cos 3(ka - \sigma t)$$
$$+g\alpha^3 k^2 \left\{ \frac{1}{16}(9T^{-1} + 18T - 27T^3)\frac{\cosh 3k(b+d)}{\cosh 3kd} \right.$$
$$-\frac{1}{16}(9T^{-2} - 5)(1 + 3T^2)\frac{\sinh 3k(b+d)}{\cosh 3kd}$$
$$\left. +\frac{1}{16}(9T^{-1} - 14T + 13T^3)\frac{\cosh k(b+d)}{\cosh kd} + \beta_{311}\frac{\sinh k(b+d)}{\cosh kd} \right\} \cos(ka - \sigma t). \tag{44}$$

where the coefficients β_{333}, β_{331}, β_{313}, β_{311}, λ_{333}, λ_{331}, λ_{313} and λ_{311} are listed as the following:

$$\beta_{333} = -\frac{1}{64}(9T^{-4} + 5T^{-2} - 53 + 39T^2) = -\lambda_{333}, \quad \beta_{331} = -\frac{1}{16}(15T^{-2} + 38 - 21T^2),$$
$$\beta_{313} = \frac{1}{48}(15T^{-2} - 34 + 19T^2), \quad \beta_{311} = \frac{1}{16}(9T^{-2} - 10 + 9T^2) = -\lambda_{311},$$
$$\lambda_{331} = \frac{1}{16}(9T^{-2} + 22 - 15T^2), \quad \lambda_{313} = -\frac{1}{16}(3T^{-2} - 6 + 3T^2).$$

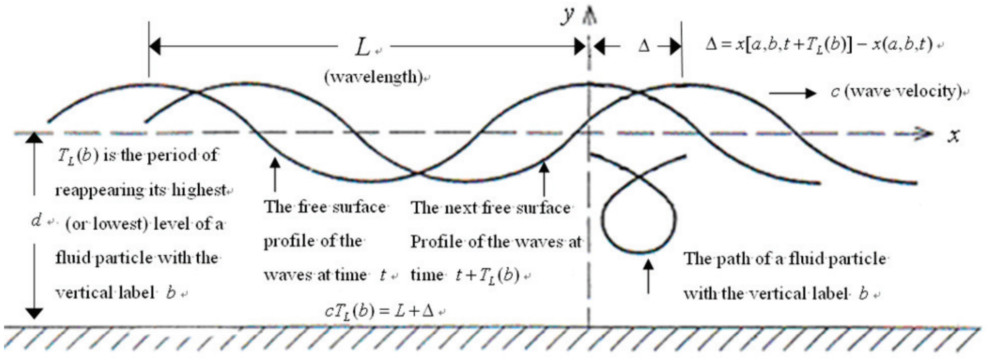

Figure 5. A sketch of the relationship between the wave velocity and particle motion (Chen 1994a).

Equation (40) is the second-order Lagrangian angular frequency σ_2 of a particle, which consists of the second-order Stokes wave angular frequency $\sigma_{w2} = \alpha^2 k^2 \sigma_0 (9T^{-2} - 10 + 9T^2)/16$ and the second-order mass-transport rate $-k\partial f_2'/\partial t$. The third-order solutions of equations (41)–(44) are periodic functions and a combination of both first and third harmonic components.

The fourth- and fifth-order solutions, including $\sigma_{3a} = \sigma_{3b} = \sigma_{4a} = 0$ and $\sigma_4 = \sigma_w 4 - k\partial f_4'/\partial t$, can be obtained by solving the non-homogeneous boundary value problems based on the solutions of previous orders. The analytical procedures are similar and the final results are listed in appendix B to be compared with those obtained by the experimental measurements. It should be pointed out that analogous to the second-order solution, the fourth-order approximation contains a time-dependent term f_4' that indicates a fourth-order correction of mass transport in the horizontal coordinate and a fourth-order vertical mean level term g_4'. Both of them exponentially decay with the depth b and are independent of the horizontal particle label a. In the fifth-order solutions, this paper provides a new fourth-order Lagrangian angular frequency term σ_4, which contains the fourth-order Stokes wave angular frequency σ_{w4} and the fourth-order mass transport rate $-k\partial f_4'/\partial t$ of the particle.

3.4. The determination of wave angular frequency $\sigma_w = ck$

The Lagrangian particle angular frequency $\sigma(b) = 2\pi/T_L(b)$ up to fifth order can be obtained as

$$\sigma = \frac{2\pi}{T_L(b)} = \sigma(b) = \sigma_0 + \sigma_2(b) + \sigma_4(b) = \sigma_w - k\frac{\partial}{\partial t}[f_2'(b, \sigma_0 t) + f_4'(b, \sigma_0 t)], \quad -d \leqslant b \leqslant 0 \tag{45}$$

Up to this point, all the properties could be found in the Lagrangian framework. The only unsolved property needing to be determined is the wave velocity $c = L/T_w$ since the wavelength L is still unknown. As shown in figure 5, for a particle marked with label (*a, b*), the motion period is $T_L(b) = 2\pi/\sigma(b)$. From the present solution, it will travel a horizontal distance after a period T_L of

$$x(a, b, t + T_L(b)) - x(a, b, t) = \left\{\frac{\partial}{\partial t}[f_2'(b, \sigma_0 t) + f_4'(b, \sigma_0 t)]\right\} T_L(b) \tag{46a}$$

and a vertical distance

$$y(a, b, t + T_L(b)) - y(a, b, t) = 0. \tag{46b}$$

During the same time interval, the next wave crest (or trough) advances a horizontal distance

$$cT_{\mathrm{L}}(b) = L + x(a, b, t + T_{\mathrm{L}}(b)) - x(a, b, t) = cT_{\mathrm{w}} + \left\{ \frac{\partial}{\partial t}[f_2'(b, \sigma_0 t) + f_4'(b, \sigma_0 t)] \right\} T_{\mathrm{L}}(b). \tag{47}$$

From this equation, the wave velocity c can be found immediately.

$$c = L/T_{\mathrm{w}} = \left\{ \frac{\partial}{\partial t}[f_2'(b, \sigma_0 t) + f_2'(b, \sigma_0 t)] \right\} \Big/ [1 - \sigma(b)/(2\pi/T_{\mathrm{w}})]. \tag{48}$$

Thus, the wave angular frequency $2\pi/T_{\mathrm{w}}$ is

$$2\pi/T_{\mathrm{w}} = \sigma(b) + k\frac{\partial}{\partial t}[f_2'(b, \sigma_0 t) + f_4'(b, \sigma_0 t)]. \tag{49}$$

This is the same as the constant term σ_{w} in the Lagrangian angular frequency $\sigma(b) = 2\pi/T_{\mathrm{w}}(b)$, which is

$$\begin{aligned}
\sigma_{\mathrm{w}} = \frac{2\pi}{T_{\mathrm{w}}} &= \sigma_0 + \frac{1}{16}\alpha^2 k^2 \sigma_0 (9T^{-2} - 10 + 9T^2) \\
&\quad + \frac{1}{1024}\alpha^4 k^4 \sigma_0 (81T^{-6} - 603T^{-4} + 3906T^{-2} - 4270 + 2477T^2 - 951T^4) \\
&= \sigma_0 + \frac{1}{64}k^2 H^2 \sigma_0 (9T^{-4} - 10T^{-2} + 9) \\
&\quad + \frac{1}{16384}k^4 H^4 \sigma_0 (-405T^{-10} - 117T^{-8} + 2454T^{-6} - 2194T^{-4} + 351T^{-2} + 39),
\end{aligned} \tag{50}$$

where σ_{w} in equation (55) is equal to the wave angular frequency obtained in the Eulerian approach (Fenton 1985).

Similarly, a general relation between the wave angular frequency σ_{w}, the Lagrangian angular frequency $\sigma(b)$ and the mass transport velocity $U_{\mathrm{M}}(b)$ of the particle motion for nonlinear water waves at a uniform depth can be also determined as

$$U_{\mathrm{M}}(b) = \sum_{n=1}^{\infty} \frac{\partial}{\partial t} f_n'(b, \sigma_0 t) = [\sigma_{\mathrm{w}} - \sigma(b)]/k. \tag{51}$$

4. Results and discussions

4.1. The particle orbits

The most important characteristic of fluid motion described by the Lagrangian solution is the particle trajectory, from which the parameter α can be determined by the wave height H, wave number k and water depth d as

$$\frac{H}{2} = [g_1 + g_3 + g_5]_{b=0, ka-\sigma t=2n\pi}, \quad n \in I. \tag{52}$$

The horizontal and vertical particle trajectories are

$$x = a + \sum_{n=1}^{5}(f_n + f_n'), \quad y = b + \sum_{n=1}^{5}(g_n + g_n'). \tag{53}$$

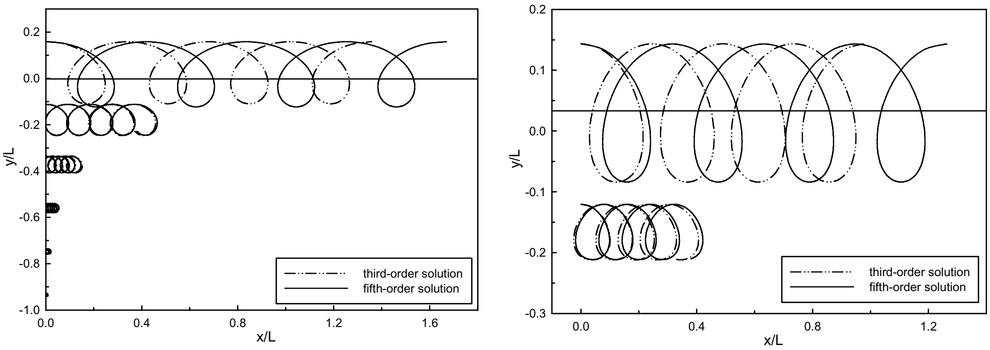

(a) (b)

Figure 6. A comparison of the third-order and fifth-order solutions for the particle trajectories at different levels b: (a) for the wave condition $d/L = \infty$ and $H/L = 0.141\,18$; and (b) for the wave condition $d/L = 0.191$ and $H/L = 0.1145$.

It is obvious that the particle orbit is not a closed curve but a spiraling-progressive curve because of the existence of a drift displacement that persists with it along the wave direction; this phenomenon is shown in figure 6. In figure 6, the particle trajectories near the highest waves in deep and finite water depths are plotted for various values of level b, including $b = 0$, which corresponds to the particles at the free surface. While the absence of a closed particle path was established for all Stokes waves (Constantin 2001a), the present approach provides an approximation for producing a quantitative estimation. It can be seen that a particle advances horizontally after each period through a distance known as the drift or mass transport in the direction of wave propagation. Near the bottom, $b = -d$, the trajectory becomes more like an ellipse because the vertical movement of the particle is less than its horizontal movement, in contrast with the trajectories near the mean still water level $b = 0$. The surface particles of the wave travel farther, and one may reasonably think that they have fewer looped structures in their particle trajectories. In fact, subsurface particles do not travel as far and have more loops because the Lagrangian particle motion period at the surface in the waves is larger than that below the surface. This also indicates that a subsurface particle takes less time to complete one period than a surface particle.

The experimental particle orbits from rest to a stable motion under the wave action are shown in figure 4. It is clearly verified that the marked particle's label (a, b) is equal to the position when the particle is initially at rest as described in equation (1). Figure 4 shows good agreement between the measured trajectories and the theoretical trajectories predicted by the proposed fifth-order Lagrangian wave theory, and demonstrates that the particles move in non-closed orbital motion and drift in the wave direction. The rightward drift is in each case greater in theory than in experiments. This may be due to the viscous effect on the particle, such that the mass transport calculated by the present theory is slightly larger than the experiment.

4.2. Velocity and pressure distribution

The velocity of any water particle marked with label (a, b) can be obtained using the present fifth-order Lagrangian solution as $\vec{V}\,(x(a,b,t),\, y(a,b,t),\, t) = \vec{i}\,x_t + \vec{j}\,y_t$. The velocity distributions along the free surface wave profiles in two different cases are shown in figure 7. For any of the 21 points (x, y) in the water, the label (a, b) is determined by the condition that the particle passes this point exactly at time t. The complete solution and the theoretical velocity

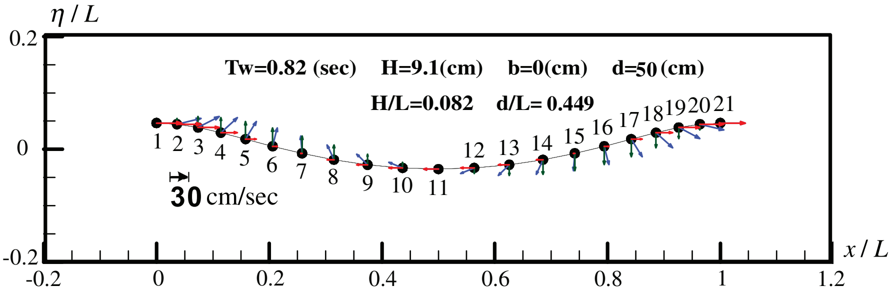

Point number		1	2	3	4	5	6	7	8	9	10	11	12	13	14	15	16	17	18	19	20	21
x/L	Exp.	0.00	0.04	0.07	0.11	0.16	0.21	0.26	0.31	0.37	0.44	0.50	0.56	0.63	0.69	0.74	0.79	0.84	0.89	0.93	0.96	1.00
	The.	0.00	0.04	0.07	0.11	0.16	0.21	0.26	0.31	0.37	0.44	0.50	0.56	0.63	0.69	0.74	0.79	0.84	0.89	0.93	0.96	1.00
η/L	Exp.	0.05	0.04	0.04	0.03	0.02	0.01	-0.01	-0.02	-0.03	-0.03	-0.04	-0.03	-0.03	-0.02	-0.01	0.01	0.02	0.03	0.04	0.04	0.05
	The.	0.05	0.04	0.04	0.03	0.02	0.01	-0.01	-0.02	-0.03	-0.03	-0.04	-0.03	-0.03	-0.02	-0.01	0.01	0.02	0.03	0.04	0.04	0.05
$u=x_t$ (cm/s)	Exp.	44.46	42.65	37.41	29.35	19.32	8.37	-2.41	-12.00	-19.52	-24.30	-25.95	-24.30	-19.52	-12.00	-2.41	8.37	19.32	29.35	37.41	42.65	44.46
	The.	44.46	42.65	37.41	29.35	19.32	8.37	-2.41	-12.00	-19.52	-24.30	-25.95	-24.30	-19.52	-12.00	-2.41	8.37	19.32	29.35	37.41	42.65	44.46
$v=y_t$ (cm/s)	Exp.	0.00	10.21	19.38	26.59	31.13	32.59	30.85	26.12	18.91	9.92	0.00	-9.92	-18.91	-26.12	-30.85	-32.59	-31.13	-26.59	-19.38	-10.21	0.00
	The.	0.00	10.21	19.38	26.59	31.13	32.59	30.85	26.12	18.91	9.92	0.00	-9.92	-18.91	-26.12	-30.85	-32.59	-31.13	-26.59	-19.38	-10.21	0.00

(a)

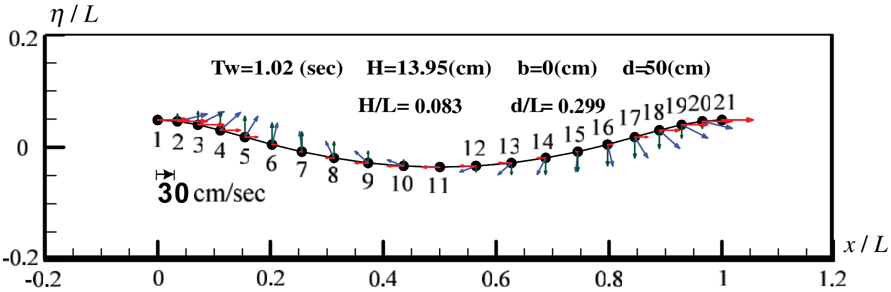

Point number		1	2	3	4	5	6	7	8	9	10	11	12	13	14	15	16	17	18	19	20	21
x/L	Exp.	0.00	0.03	0.07	0.11	0.15	0.20	0.26	0.31	0.37	0.44	0.50	0.56	0.63	0.69	0.74	0.80	0.85	0.89	0.93	0.97	1.00
	The.	0.00	0.03	0.07	0.11	0.15	0.20	0.26	0.31	0.37	0.44	0.50	0.56	0.63	0.69	0.74	0.80	0.85	0.89	0.93	0.97	1.00
η/L	Exp.	0.05	0.05	0.04	0.03	0.02	0.01	-0.01	-0.02	-0.03	-0.03	-0.04	-0.03	-0.03	-0.02	-0.01	0.01	0.02	0.03	0.04	0.05	0.05
	The.	0.05	0.05	0.04	0.03	0.02	0.01	-0.01	-0.02	-0.03	-0.03	-0.04	-0.03	-0.03	-0.02	-0.01	0.01	0.02	0.03	0.04	0.05	0.05
$u=x_t$ (cm/s)	Exp.	58.30	55.81	48.66	37.73	24.33	9.99	-3.77	-15.64	-24.67	-30.28	-32.17	-30.28	-24.67	-15.64	-3.77	9.99	24.33	37.73	48.66	55.81	58.30
	The.	58.30	55.81	48.66	37.73	24.33	9.99	-3.77	-15.64	-24.67	-30.28	-32.17	-30.28	-24.67	-15.64	-3.77	9.99	24.33	37.73	48.66	55.81	58.30
$v=y_t$ (cm/s)	Exp.	0.00	13.20	24.91	33.83	39.03	40.08	37.12	30.72	21.79	11.26	0.00	-11.26	-21.79	-30.72	-37.12	-40.08	-39.03	-33.83	-24.91	-13.20	0.00
	The.	0.00	13.20	24.91	33.83	39.03	40.08	37.12	30.72	21.79	11.26	0.00	-11.26	-21.79	-30.72	-37.12	-40.08	-39.03	-33.83	-24.91	-13.20	0.00

(b)

Figure 7. Comparisons between the velocity distributions obtained by the presented theory and those from the experimental PS motion measurements along the free surface wave profiles in two large experimental waves cases, where the time interval between two consecutive points (•) is $T_{\mathrm{w}}/20$ and T_{w} is the wave period. The table under the figure denotes the corresponding experimental (Exp.) and theoretical (The.) values at the points (no. 1–21) in the figure.

$\vec{V} = \vec{i}\,x_t + \vec{j}\,y_t$ are obtained after the label (a, b) is substituted into the solution. The velocity distribution is in good agreement with the experiments along the free surface, as is shown in figure 7. Figure 8 illustrates the theoretical and experimental results of the dimensionless extremes (positive and negative maximum) for horizontal and vertical velocity components ku_g/σ_0, ku_s/σ_0, kv_g/σ_0 and kv_s/σ_0 of particles with various relative water depths (d/L) and wave steepnesses (H/L). The dimensionless horizontal and vertical velocities increase as the wave steepness increases but decrease as the relative water depth increases. The water pressure distribution can also be depicted as shown in figure 9. Good correspondence is seen between the present fifth-order solution and experimental data under the wave crest and trough. These results are in accord with the linearized analysis of Escher and Schlurmann (2008) and the recent investigation on the pressure beneath waves of large amplitude by Constantin and Strauss (2010).

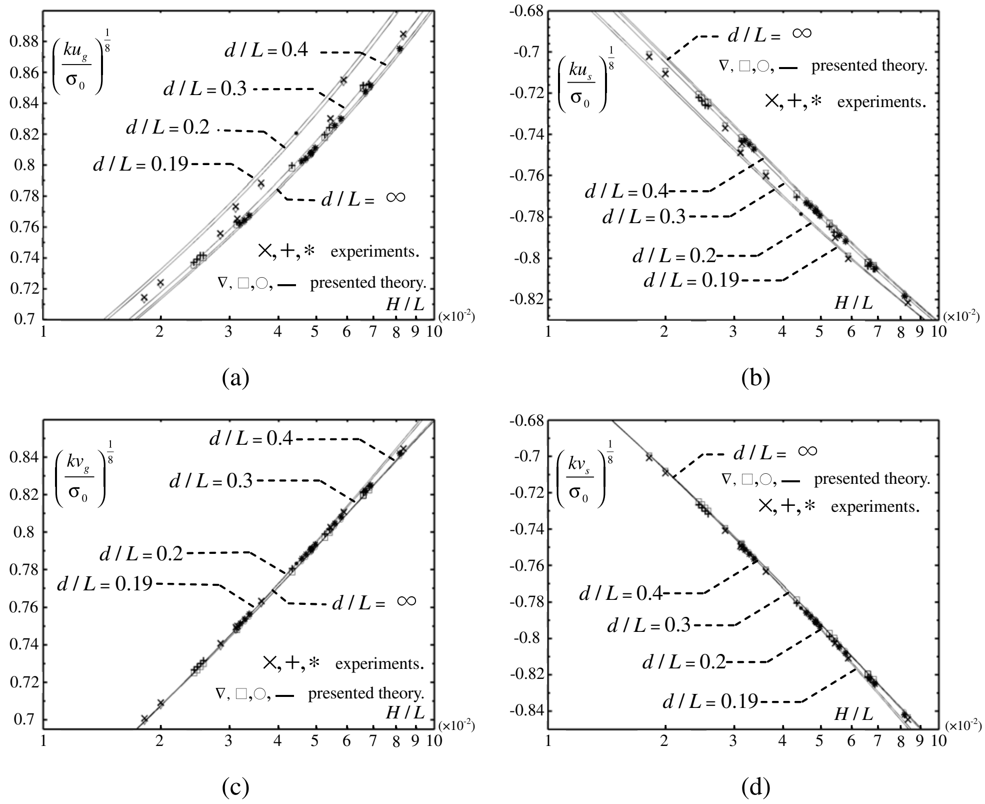

Figure 8. Comparisons between the results obtained by the presented theory and those obtained from the experimental PS motion measurements in the considered waves for the relations of the dimensionless extreme (positive and negative maximum) horizontal and vertical components (a) ku_g/σ_0, (b) ku_s/σ_0, (c) kv_g/σ_0 and (d) kv_s/σ_0 in the experimental wave cases with the relative water depth d/L and wave steepness H/L, where $u_g = (x_t)_g$ is the positive maximum horizontal velocity component, $u_s = (x_t)_s$ is the negative maximum horizontal velocity component, $v_g = (y_t)_g$ is the positive maximum vertical velocity component, and $v_s = (y_t)_s$ is the negative maximum vertical velocity component. While the symbols $\times$ and ∇ are the experimental and theoretical values between the relative water depth $d/L = 0.2$ and 0.3, + and □ are those between $d/L = 0.3$ and 0.4, * and ○ are those between $d/L = 0.4$ and ∞, and • is that around $d/L = 0.19$. These symbols have the same meaning as in figures 8–11.

4.3. Mass transport velocity and mean wave momentum

Up to the fifth order, using equation (51) the forward mass transport velocity $U_{\mathrm{M}}(b)$ of the particle along the wave direction yields

$$U_{\mathrm{M}}(b) = \frac{\partial}{\partial t}[f_2'(b, \sigma_0 t) + f_4'(b, \sigma_0 t)] = [\sigma_{\mathrm{w}} - \sigma(b)]/k = \left[1 - \frac{T_{\mathrm{w}}}{T_{\mathrm{L}}(b)}\right] c. \tag{54}$$

The first term of equation (54) on the right-hand side, a second-order quantity $\partial f_2'/\partial t$, is the same as that obtained by Longuet-Higgins (1987). From equation (54), the mass transport velocity increases only with wave steepness as a function of the water depth d and level b. Differentiating equation (54) with respect to b shows that the mass transport velocity is always positive but experiences exponential decay from the surface to the bottom. The experimental and theoretical results for the mass transport velocity kU_{M}/σ_0 and the

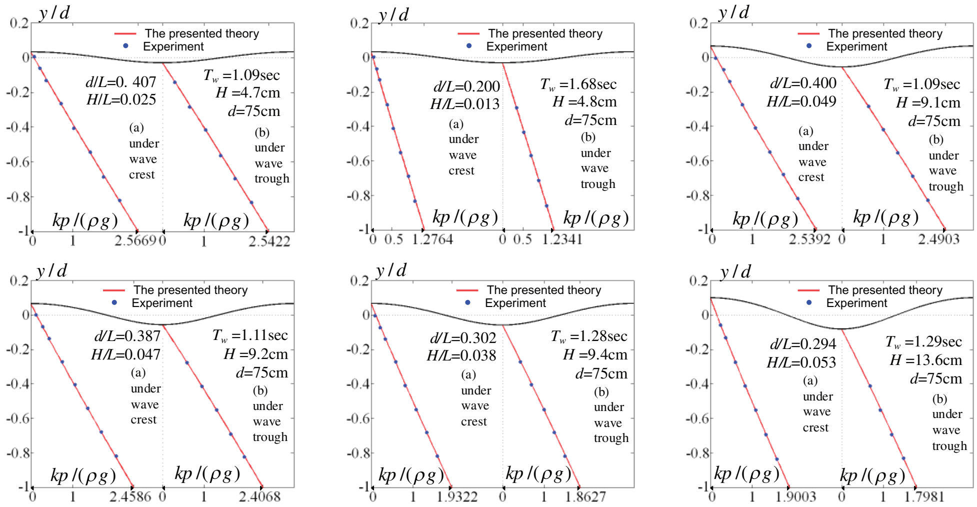

Figure 9. The dimensionless total pressure distributions under the wave crest and wave trough.

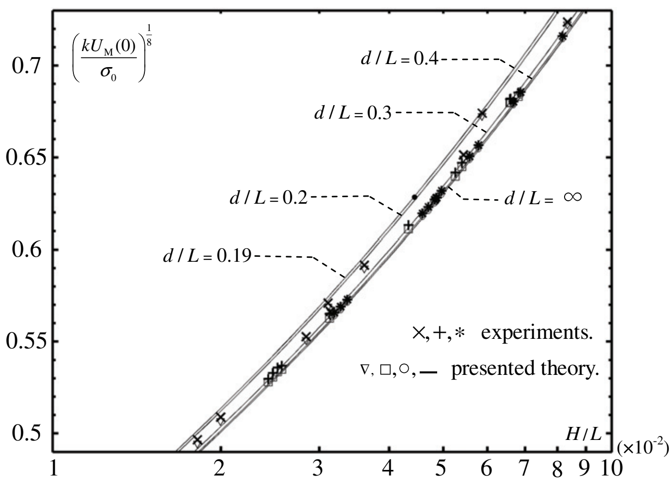

Figure 10. Comparison of the dimensionless mass transport particle velocity $kU_{\mathrm{M}}(0)/\sigma_0$ at the free surface with the relative water depth d/L and the wave steepness H/L.

difference $(T_{\mathrm{L}} - T_{\mathrm{w}})/T_{\mathrm{w}}$ for particles at the free surfaces $b = 0$ in the considered waves are shown in figures 10 and 11, respectively; both increase as the wave steepness H/L increases but decrease as the relative water depth d/L increases. The mean wave momentum M at a wavelength L can obviously be calculated from the motion of particles described in the Lagrangian approach as presented, which is easier than that in the Eulerian approach:

$$M = \frac{\rho}{L}\int_0^L \int_{-d}^{\eta} u(x, y, t)\,\mathrm{d}y\,\mathrm{d}x = \frac{\rho}{L}\int_0^L \int_{-d}^{0} u(a, b, t)\frac{\partial(x, y)}{\partial(a, b)}\,\mathrm{d}b\,\mathrm{d}a$$

$$= \frac{\rho}{L}\int_0^L \int_{-d}^{0} x_t(a, b, t)\,\mathrm{d}b\,\mathrm{d}a = \rho\int_{-d}^{0} U_m(b)\,\mathrm{d}b. \tag{55}$$

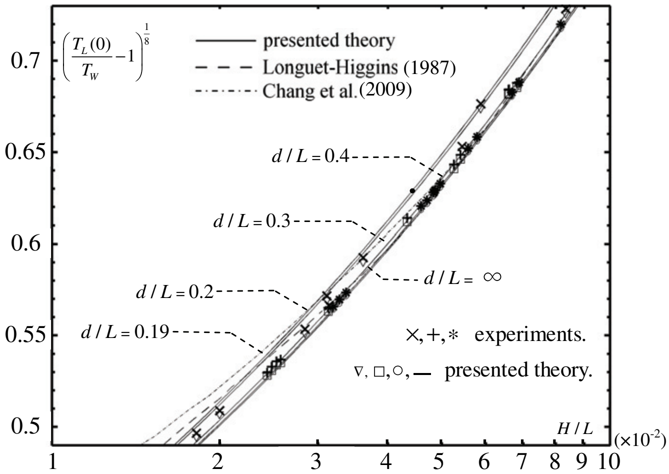

Figure 11. Comparison of the nondimensional difference $[T_{\rm L}(0) - T_{\rm w}]/T_{\rm w}$ of particles at the free surface with the relative water depth d/L and the wave steepness H/L; $T_{\rm L}(0)$ is the particle motion period at the free surface and $T_{\rm w}$ is the wave period. The result of Chang *et al* (2009) used the Eulerian approach numerical model by Reinecker and Fenton (1981) by taking the $N = 32$ term for the deep water waves.

4.4. Lagrangian mean level of particle motion

In addition to the mass transport velocity, a new term $\sum g_n'$, called the Lagrangian mean level, encompassing the time average of the particle motion period $T_{\rm L}$ or the wavelength average with label a, is also included in the present solution. However, the physical or mathematical meaning of this term has not been found yet. To give a clear explanation of the Lagrangian mean level, the derivation is given below. By applying equations (1*a*) and (1*b*) and taking $b = $ const at time $t = $ const as well as using equation (53), we have

$$b = \frac{1}{L}\int_x^{x+L} y(a,b,t)\,\mathrm{d}x(a,b,t) = \frac{1}{L}\int_a^{a+L}\left[b+\sum_{n=1}^{\infty}(g_n+g_n')\right]\left[1+\sum_{n=1}^{\infty}\frac{\partial f_n}{\partial a}\right]\mathrm{d}a$$

$$= b+\sum_{n=1}^{\infty} g_n' + \frac{1}{L}\int_a^{a+L}\left(\sum_{n=1}^{\infty} g_n\right)\left(\sum_{n=1}^{\infty}\frac{\partial f_n}{\partial a}\right)\mathrm{d}a, \tag{56}$$

where both b and t are constants.

Thus, the Lagrangian mean level up to a fifth-order solution can be obtained as

$$g_1' = g_3' = g_5' = 0, \quad g_2' = -\frac{1}{L}\int_a^{a+L} g_1\frac{\partial f_1}{\partial a}\,\mathrm{d}a \quad \text{and}$$
$$g_4' = -\frac{1}{L}\int_a^{a+L}\left(g_1\frac{\partial f_3}{\partial a}+g_2\frac{\partial f_2}{\partial a}+g_3\frac{\partial f_1}{\partial a}\right)\mathrm{d}a. \tag{57}$$

These results are the same as those obtained in the present fifth-order Lagrangian solution.

Taking the average particle's elevation up to the fifth order over the period $T_{\rm L}(b)$ of a particle motion or wavelength L in label a, the present theory gives the Lagrangian mean level

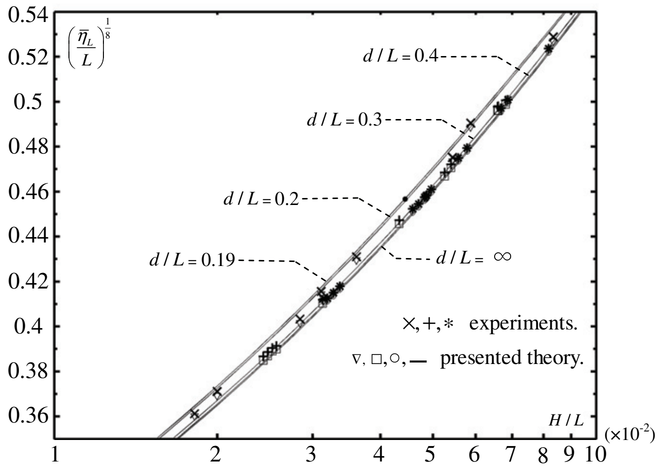

Figure 12. Comparison of the dimensionless Lagrangian mean particle level $\bar{\eta}_{\mathrm{L}}(0)/L$ at the free surface with the relative water depth d/L and the wave steepness H/L.

$\bar{\eta}_{\mathrm{L}}(b)$, which is higher than the Eulerian mean level $\bar{\eta}_{\mathrm{w}} = 0$ at the free surface.

$$\bar{\eta}_{\mathrm{L}}(b) = \frac{1}{T_{\mathrm{L}}}\int_0^{T_{\mathrm{L}}} (y-b)\,\mathrm{d}t = g_2' + g_4' \neq \frac{1}{T_{\mathrm{w}}}\int_0^{T_{\mathrm{w}}} (y-b)\,\mathrm{d}t. \tag{58}$$

Longuet-Higgins (1986, 1987) also showed that the Lagrangian mean level is higher than the Eulerian mean level. However, this expression is only applicable to the particles at the free surface and is the same as that given by the first term of equation (58) at $b = 0$. The experimental and theoretical results for $\bar{\eta}_{\mathrm{L}}/L$ of particles at the free surface $b = 0$ are shown in figure 12, which indicates that the Lagrangian mean level increases as the wave steepness H/L increases but decreases as the relative water depth d/L increases.

5. Concluding remarks

With a set of careful quantitative measurements of the trajectories of particles in irrotational finite-amplitude progressive gravity water waves at a uniform depth, a simple definition of the Lagrangian labels marked with the particle is given. Then, the fifth-order Lagrangian solutions satisfying all the governing equations and the boundary conditions in a Lagrangian framework are derived. The Lagrangian fifth-order solution not only determines all the wave properties revealed in the Eulerian solution, but also extends further to obtain the particle trajectory, the Lagrangian wave period, the mass transport and the Lagrangian mean level, which are excluded from the Eulerian system. The Lagrangian solution is able to obtain the wave velocity or the nonlinear dispersion relation from the particle motion independently and is equal to that of the Eulerian solution. Consequently, it gives a general relation that is a function of only the mean level $\bar{y} = b$ between the wave angular frequency, the Lagrangian angular frequency and the mass transport velocity of a particle in the waves. The Lagrangian mean particle level of motion–orbit that is only a function of b due to particle deformations marked with the Lagrangian labels (a, b) under the conservation of mass has been expressed formulaically.

The angular frequency of the particle motion differs from the Eulerian wave frequency. It is only a function of the marked label b of each individual particle and can be obtained immediately at each odd-order solution. The fifth-order particle motion period gives accurate results near the limiting wave when compared to those at the free surface given by Longuet-Higgins (1986) and Chang *et al* (2009), which are derived from the Eulerian–Lagrangian approach that only applies to particles at the free surface.

As can be seen from the second- and fourth-order solutions, the Lagrangian mean level of gravity waves is higher than the Eulerian mean level at the free surface as was noted by Longuet-Higgins (1986). Time-dependent terms related to the mass transport velocity expressed as a function of only its vertical label b are obtained to the fifth order. This drift velocity is always positive but monotonically decays from the surface to the bottom. This implies that the particles move forward a longer horizontal displacement at the surface in each complete orbit and the wave's subsurface particles travel less far and slower. The mean wave momentum with the same result as that of the Eulerian solution is exhibited by integrating all the particle mass transport velocities.

Finally, a set of experiments measuring the Lagrangian properties of nonlinear progressive water waves is conducted in a wave tank. From these experimental results, the marked particle labels (a, b) are verified to be equal to the particle position in still water and show good agreement between the measured trajectories and the theoretical trajectories predicted by the proposed fifth-order Lagrangian solution. The close correspondence also extends to the wave profile, the velocities, the wave pressure, the periods, the mass transport velocities and the Lagrangian mean levels of the particles obtained in this solution and demonstrates that the non-dimensional motion period, mass transport velocity, Lagrangian mean level, and extreme horizontal and vertical velocity components of water particles in the waves all increase as the wave steepness increases but decrease as the relative water depth increases.

Acknowledgments

We thank Mr Meng-Syue Li and Mr Jheng-Da Li who performed the experimental work presented here. We also thank the Water Resources Agency, Taiwan, for providing funding under grant number MOEAWRA 0970305.

Appendix A. The energy equation, the potential function and the irrotational condition in Lagrangian form

The dynamic equations in a Lagrangian description can be deduced from Newton's second law of motion for incompressible and inviscid flow (Lamb 1932, Miche 1944, Chen 1994):

$$x_{tt}x_a + y_{tt}y_a = -gy_a - \frac{1}{\rho}P_a, \tag{A.1a}$$

$$x_{tt}x_b + y_{tt}y_b = -gy_b - \frac{1}{\rho}P_b, \tag{A.1b}$$

Equations (A.1a) and (A.1b) can be integrated over time between the limits 0 and t to give

$$x_t x_a + y_t y_a - (x_t x_a + y_t y_a)_{t=0} = -\frac{\partial K}{\partial a}, \tag{A.2a}$$

$$x_t x_b + y_t y_b - (x_t x_b + y_t y_b)_{t=0} = -\frac{\partial K}{\partial b}, \tag{A.2b}$$

$$\int \frac{\mathrm{d}P}{\rho} + gy - K_t - \frac{1}{2}(x_t^2 + y_t^2) = 0, \tag{A.2c}$$

where

$$K(a, b, t) = \int_0^t \left[\int \frac{\mathrm{d}P}{\rho} + gy - \frac{1}{2}(x_t^2 + y_t^2) \right] \mathrm{d}t.$$

Equation (A.2) is usually called Weber's transformation (Lamb 1932), and (A.2*c*) is the energy equation for an ideal fluid in the Lagrangian system. When taking (a, b) as the initial particle position at the initial time $t = 0$, equations (A.2*a*)–(A.2*c*) are consistent with equations (2) and (3) in Art. 14 of Lamb (1932).

Let the instant of time at which the velocity potential ϕ_0 exists be taken as the origin of time $t = 0$; then

$$(u\delta x + v\delta y)_{t=0} = [(x_t x_a + y_t y_a)\delta a + (x_t x_b + y_t y_b)\delta b]_{t=0} = \delta\phi_0. \tag{A.3}$$

By multiplying (A.2*a*) and (A.2*b*) by the Lagrangian variables δa and δb and adding, we obtain

$$(x_t x_a + y_t y_a)\delta a + (x_t x_b + y_t y_b)\delta b = (\delta\phi_0 - \delta K) = \delta\phi = \frac{\partial\phi}{\partial a}\delta a + \frac{\partial\phi}{\partial b}\delta b, \tag{A.4}$$

where ϕ is the velocity potential at time t under the same portion of the fluid in which ϕ_0 exists at initial time $t = 0$. When taking (a, b) as the initial particle position at the initial time $t = 0$, equation (A.4) is consistent with the third equation in Art. 17 of Lamb (1932). Thus, $\phi = \phi(a, b, t)$ with

$$\frac{\partial\phi}{\partial a} = (x_t x_a + y_t y_a), \qquad \frac{\partial\phi}{\partial b} = (x_t x_b + y_t y_b). \tag{A.5}$$

The relations (A.5) explicitly define the velocity potential in Lagrangian representation. By cross-differentiation of (A.5) following the order δb, δa, we obtain the irrotational flow condition in Lagrangian coordinates

$$x_{at}x_b - x_{bt}x_a + y_{at}y_b - y_{bt}y_a = \frac{\partial(x_t, x)}{\partial(a, b)} + \frac{\partial(y_t, y)}{\partial(a, b)} = 0. \tag{A.6}$$

Equation (A.6) is the same as the vorticity conservation for irrotational motion obtained by Miche (1944) and Yakubovich and Zenkovich (2001).

Appendix B. Lagrangian fourth- and fifth-order solutions

Following the same derivation procedures as the third-order solution, the fourth- and fifth-order solutions of particle trajectories, velocity potential and pressure in Lagrangian form are

$$f_n = \alpha^n k^{n-1} \sum_{i=0}^{n} \sum_{j=1}^{n} \beta_{nij} \frac{\cosh ik(b+d)}{\cosh ikd} \sin j(ka - \sigma t),$$

$$f_n' = \alpha^n k^{n-1} \sum_{i=1}^{n} m_{ni} \frac{\cosh ik(b+d)}{\cosh ikd} \sigma_0 t, \qquad f_5' = 0, n = 4, 5$$

$$\beta_{444} = -(5 + T^2)^{-1}(405T^{-6} + 756T^{-4} - 7623T^{-2} + 9872 - 1481T^2$$
$$-1732T^4 - 197T^6)/1536, \qquad T = \tanh kd,$$

$$\beta_{442} = (-135T^{-4} - 552T^{-2} + 1298 - 432T^2 - 115T^4)/384,$$
$$\beta_{424} = (135T^{-4} - 390T^{-2} + 128 + 390T^2 - 263T^4)/768,$$
$$\beta_{422} = (81T^{-6} + 297T^{-4} - 654T^{-2} - 358 + 381T^2 - 131T^4)/768,$$
$$\beta_{404} = (27T^{-4} - 156T^{-2} + 314 - 268T^2 + 83T^4)/384,$$
$$\beta_{402} = (-21T^{-4} + 41 - 43T^2 + 23T^4)/96,$$
$$\beta_{555} = -(25 + 20T^2 + 3T^4)^{-1}(2025T^{-8} + 8370T^{-6} - 88578T^{-4} + 135290T^{-2}$$
$$+28240 - 121450T^2 - 2142T^4 + 32830T^6 + 5415T^8)/4096,$$
$$\beta_{553} = (5 + T^2)^{-1}(-2295T^{-6} - 14274T^{-4} + 66439T^{-2} - 43332$$
$$-26017T^2 + 16070T^4 + 3665T^6)/3072,$$
$$\beta_{551} = (-351T^{-6} - 3993T^{-4} - 5942T^{-2} + 3782 + 885T^2 - 1165T^4)/1024,$$
$$\beta_{535} = (5 + T^2)^{-1}(6885T^{-6} - 18783T^{-4} - 41718T^{-2} + 171938 - 164407T^2$$
$$+32093T^4 + 13992T^6)/15360,$$
$$\beta_{533} = (5 + T^2)^{-1}(1215T^{-8} + 5913T^{-6} - 13005T^{-4} - 41323T^{-2}$$
$$+53949 - 2901T^2 - 5551T^4 - 345T^6)/4096,$$
$$\beta_{531} = (405T^{-6} + 3933T^{-4} - 222T^{-2} - 18266 + 19169T^2 - 4251T^4)/1536,$$
$$\beta_{515} = (1053T^{-6} - 8982T^{-4} + 27798T^{-2} - 40208 + 27685T^2 - 7346T^4)/15360,$$
$$\beta_{513} = (-270T^{-6} + 9T^{-4} + 2920T^{-2} - 4946 + 3470T^2 - 1183T^4)/3072,$$
$$\beta_{511} = (243T^{-6} - 2781T^{-4} + 13494T^{-2} - 14930 + 8695T^2$$
$$-3569T^4)/3072, \quad \text{elsewhere zero},$$
$$m_{44} = (9T^{-4} + 60T^{-2} + 38 - 36T^2 - 7T^4)/32,$$
$$m_{42} = (-15T^{-2} + 11 + 7T^2 - 19T^4)/32, \quad \text{elsewhere zero},$$
$$g_n = \alpha^n k^{n-1} \sum_{i=1}^{n} \sum_{j=1}^{n} \lambda_{nij} \frac{\sinh ik(b+d)}{\cosh ikd} \cos j(ka - \sigma t),$$
$$g'_n = \alpha^n k^{n-1} \sum_{i=1}^{n} l_{ni} \frac{\sinh ik(b+d)}{\cosh ikd}, \quad g'_5 = 0, n = 4, 5$$
$$\lambda_{444} = -\beta_{444}, \quad \lambda_{555} = -\beta_{555},$$
$$\lambda_{442} = (27T^{-4} + 105T^{-2} - 289 + 99T^2 + 26T^4)/96,$$
$$\lambda_{553} = (5 + T^2)^{-1}(675T^{-6} + 4050T^{-4} - 20827T^{-2} + 13924 + 8197T^2$$
$$-5110T^4 - 1165T^6)/1024,$$
$$\lambda_{551} = (135T^{-6} + 1677T^{-4} + 3478T^{-2} - 2862 - 605T^2 + 865T^4)/1024,$$
$$\lambda_{535} = (5 + T^2)^{-1}(-405T^{-6} + 1029T^{-4} + 2500T^{-2} - 9590 + 8851T^2$$
$$-1674T^4 - 738T^6)/1024,$$
$$\lambda_{533} = (5 + T^2)^{-1}(-1215T^{-8} - 5913T^{-6} + 16245T^{-4} + 40051T^{-2}$$
$$-77293 + 30629T^2 + 1335T^4 - 1791T^6)/4096,$$

$$\lambda_{531} = (-81T^{-6} - 777T^{-4} + 110T^{-2} + 3706 - 3957T^2 + 999T^4)/512,$$
$$\lambda_{515} = (-27T^{-6} + 216T^{-4} - 642T^{-2} + 900 - 603T^2 + 156T^4)/1024,$$
$$\lambda_{513} = (54T^{-6} + 297T^{-4} - 1616T^{-2} + 2334 - 1406T^2 + 337T^4)/1024,$$
$$\lambda_{511} = (-243T^{-6} + 2205T^{-4} - 11286T^{-2} + 11890 - 6935T^2 + 3217T^4)/3072, \quad \text{elsewhere zero},$$
$$l_{44} = (9T^{-4} + 84T^{-2} + 174 - 60T^2 - 15T^4)/128,$$
$$l_{42} = (-15T^{-2} + 5 + 7T^2 - 13T^4)/32, \quad \text{elsewhere zero},$$
$$\phi_n = \alpha^n k^{n-2}\sigma_0 \sum_{i=0}^{n}\sum_{j=1}^{n} \gamma_{nij} \frac{\cosh ik(b+d)}{\cosh ikd} \sin j(ka - \sigma t),\ n = 4, 5,$$
$$\gamma_{444} = -\beta_{444}, \quad \gamma_{442} = (27T^{-4} + 78T^{-2} - 436 + 162T^2 + 41T^4)/192,$$
$$\gamma_{424} = (-27T^{-4} + 87T^{-2} - 37 - 87T^2 + 64T^4)/96,$$
$$\gamma_{422} = (-81T^{-6} - 135T^{-4} + 474T^{-2} + 454 - 201T^2 - 127T^4)/768,$$
$$\gamma_{404} = (-27T^{-4} + 168T^{-2} - 358 + 320T^2 - 103T^4)/192,$$
$$\gamma_{402} = (3T^{-2} - 5 + 7T^2 - 5T^4)/24, \quad \text{elsewhere zero},$$
$$\phi_4' = \alpha^4 k^2 \sigma_0^2 (-9T^{-4} + 36T^{-2} - 62 + 52T^2 - 17T^4)t/64, \quad \phi_5' = 0,$$
$$\gamma_{555} = -\beta_{555}, \quad \gamma_{553} = (5 + T^2)^{-1}(405T^{-6} + 1926T^{-4} - 16869T^{-2} + 12364 + 6771T^2 - 4370T^4 - 995T^6)/1024,$$
$$\gamma_{551} = (27T^{-6} + 357T^{-4} + 782T^{-2} - 1710 - 265T^2 + 425T^4)/1024,$$
$$\gamma_{535} = (5 + T^2)^{-1}(-2025T^{-6} + 6435T^{-4} + 11718T^{-2} - 56858 + 58195T^2 - 12329T^4 - 5136T^6)/3072,$$
$$\gamma_{533} = (5 + T^2)^{-1}(-1215T^{-8} - 4293T^{-6} + 12429T^{-4} + 39903T^{-2} - 25437 - 41967T^2 + 17807T^4 + 4821T^6)/4096,$$
$$\gamma_{531} = (-81T^{-6} - 639T^{-4} + 54T^{-2} + 2854 - 2317T^2 + 897T^4)/1536,$$
$$\gamma_{515} = (-405T^{-6} + 3762T^{-4} - 12438T^{-2} + 18968 - 13645T^2 + 3758T^4)/3072,$$
$$\gamma_{513} = (162T^{-6} - 207T^{-4} - 1128T^{-2} + 1966 - 1170T^2 + 377T^4)/1024, \quad \text{elsewhere zero},$$
$$\frac{P_n}{\rho} = g\alpha^n k^{n-1} \sum_{i=0}^{n}\sum_{j=0}^{n} \left[C_{nij} \frac{\cosh ik(b+d)}{\cosh ikd} + S_{nij} \frac{\sinh ik(b+d)}{\cosh ikd} \right] \cos j(ka - \sigma t), \quad n = 4, 5,$$
$$C_{444} = -4T\beta_{444}, \quad S_{444} = \beta_{444},$$
$$C_{424} = (-351T^{-3} + 1086T^{-1} - 424T - 1086T^3 + 775T^5)/384,$$
$$S_{424} = (9T^{-4} - 24T^{-2} + 6 + 24T^2 - 15T^4)/64,$$
$$C_{404} = (-81T^{-3} + 492T^{-1} - 1030T + 908T^3 - 289T^5)/192,$$
$$C_{442} = (189T^{-3} + 636T^{-1} - 2530T + 1116T^3 + 269T^5)/384,$$
$$S_{442} = (-27T^{-4} - 105T^{-2} + 289 - 99T^2 - 26T^4)/96,$$
$$C_{422} = (-81T^{-5} + 27T^{-3} + 294T^{-1} + 550T - 21T^3 - 385T^5)/384,$$

$S_{422} = (27T^{-6} + 99T^{-4} - 346T^{-2} - 66 + 255T^{2} - 97T^{4})/256,$

$C_{402} = (-39T^{-1} + 107T - 97T^{3} + 29T^{5})/96,$

$C_{440} = (9T^{-3} + 60T^{-1} + 38T - 36T^{3} - 7T^{5})/64,$

$S_{440} = (-9T^{-4} - 84T^{-2} - 174 + 60T^{2} + 15T^{4})/128,$

$C_{420} = (-3T^{-1} + 5T + 3T^{3} - 5T^{5})/32,$

$S_{420} = (15T^{-2} - 5 - 7T^{2} + 13T^{4})/32,$

$C_{400} = (9T^{-3} - 36T^{-1} + 62T - 52T^{3} + 17T^{5})/64,$ elsewhere zero,

$C_{555} = -5T\beta_{555};\ S_{555} = \beta_{555},$

$$C_{535} = (5+T^{2})^{-1}(-2835T^{-5} + 8493T^{-3} + 16718T^{-1} - 76038T + 75897T^{3} - 15623T^{5} - 6612T^{7})/1024,$$

$$S_{535} = (5+T^{2})^{-1}(405T^{-6} - 1029T^{-4} - 2500T^{-2} + 9590 - 8851T^{2} + 1647T^{4} + 738T^{6})/1024,$$

$C_{515} = (-513T^{-5} + 4632T^{-3} - 14998T^{-1} + 22508T - 15985T^{3} + 4356T^{5})/1024,$

$S_{515} = (27T^{-6} - 216T^{-4} + 642T^{-2} - 900 + 603T^{2} - 156T^{4})/1024,$

$$C_{553} = (5+T^{2})^{-1}(1755T^{-5} + 9486T^{-3} - 62711T^{-1} + 491116T + 23909T^{3} - 18730T^{5} - 4105T^{7})/1024,$$

$$S_{553} = (5+T^{2})^{-1}(-675T^{-6} - 4050T^{-4} + 20827T^{-2} - 13924 - 8197T^{2} + 5110T^{4} + 1165T^{6})/1024,$$

$$C_{533} = (5+T^{2})^{-1}(-3645T^{-7} - 8019T^{-5} + 35559T^{-3} + 87609T^{-1} - 38263T - 157849T^{3} + 71117T^{5} + 19635T^{7})/4096,$$

$$S_{533} = (5+T^{2})^{-1}(1215T^{-8} + 5913T^{-6} - 16245T^{-4} - 40051T^{-2} + 77293 - 30629T^{2} - 1335T^{4} + 1791T^{6})/4096,$$

$C_{513} = (378T^{-5} - 1449T^{-3} + 1216T^{-1} - 1598T + 2302T^{3} - 849T^{5})/1024,$

$S_{513} = (-54T^{-6} - 297T^{-4} + 1616T^{-2} - 2334 + 1406T^{2} - 337T^{4})/1024,$

$C_{551} = (189T^{-5} + 2031T^{-3} + 1682T^{-1} - 5674T + 145T^{3} + 1755T^{5})/1024,$

$S_{551} = (-135T^{-6} - 1677T^{-4} - 3478T^{-2} + 2862 + 605T^{2} - 865T^{4})/1024,$

$C_{531} = (-81T^{-5} - 537T^{-3} + 382T^{-1} + 2866T - 2549T^{3} + 687T^{5})/512,$

$S_{531} = (81T^{-6} + 777T^{-4} - 110T^{-2} - 3706 + 3957T^{2} - 999T^{4})/512,$

$C_{511} = (243T^{-5} - 1809T^{-3} + 12198T^{-1} - 14186T + 9127T^{3} - 3653T^{5})/3072,$

$S_{511} = (243T^{-6} - 2205T^{-4} + 11286T^{-2} - 11890 + 6935T^{2} - 3217T^{4})/3072,$ elsewhere zero,

$$\sigma_4 = \alpha^4 k^4 \left[-m_{44}\frac{\cosh 4k(b+d)}{\cosh 4kd} - m_{42}\frac{\cosh 2k(b+d)}{\cosh 2kd} + \frac{1}{1024}(81T^{-6} - 603T^{-4} + 3906T^{-2} - 4270 + 2477T^{2} - 951T^{4}) \right]\sigma_0$$

References

Biesel F 1952 Study of wave propagation in water of gradually varying depth *Gravity Waves* NBS Circular 521 (Washington, DC: US National Bureau of Standards) pp 243–53

Buldakov E V, Taylor P H and Taylor R E 2006 New asymptotic description of nonlinear water waves in Lagrangian coordinates *J. Fluid Mech.* **562** 431–44

Chang H K, Chen Y Y and Liou J C 2009 Particle trajectories of nonlinear gravity waves in deep water *Ocean Eng.* **36** 324–9

Chang H K, Liou J C and Su M Y 2007 Particle trajectory and mass transport of finite-amplitude waves in water of uniform depth *Eur. J. Mech.* B **26** 385–403

Chen Y Y 1994a Perturbation analysis of irrotational progressive gravity waves in fluid of any uniform depth in Lagrangian form *Proc. 16th Conf. on Ocean Eng.* (*Taiwan*) pp 1–29 (in Chinese)

Chen Y Y 1994b Perturbation analysis of irrotational standing waves in fluid of any uniform depth in Lagrangian form *Proc. 16th Conf. on Ocean Eng.* (*Taiwan*) pp 30–59 (in Chinese)

Chen Y Y and Hsu H C 2009a The transformation between the Eulerian and Lagrangian solutions for irrotational progressive water waves *Acta Phys. Sin.* **58** 40–9 (in Chinese)

Chen Y Y and Hsu H C 2009b Third-order asymptotic solution of nonlinear standing water waves in Lagrangian coordinates *Chin. Phys.* B **18** 861–71

Chen Y Y, Hsu H C, Chen G Y and Hwung H H 2006 Theoretical analysis of surface waves shoaling and on a sloping bottom. Part 2: Nonlinear waves *Wave Motion* **43** 339–56

Clamond D 2007 On the Lagrangian description of steady surface gravity waves *J. Fluid Mech.* **589** 433–54

Cokelet E D 1977 Steep gravity waves in water of arbitrary uniform depth *Phil. Trans. R. Soc.* A **286** 183–230

Constantin A 2001a On the deep water wave motion *J. Phys. A: Math. Gen.* **34** 1405–17

Constantin A 2001b Edge waves along a sloping beach *J. Phys. A: Math. Gen.* **34** 9723–31

Constantin A 2006 The trajectories of particles in Stokes waves *Inv. Math.* **166** 523–35

Constantin A, Ehrnstrom M and Wahlen E 2007 Symmetry of steady periodic gravity water waves with vorticity *Duke Math. J.* **140** 591–603

Constantin A and Escher J 2007 Particle trajectories in solitary water waves *Bull. Am. Math. Soc.* **44** 423–31

Constantin A and Strauss W 2010 Pressure beneath a Stokes wave *Commun. Pure Appl. Math.* **64** 533–57

Davies A G and Heathershaw A D 1984 Surface-wave propagation over sinusoidally varying topography *J. Fluid Mech.* **144** 419–43

Escher J and Schlurmann T 2008 On the recovery of the free surface from the pressure within periodic traveling water waves *J. Nonlinear Math. Phys.* **15** 50–7

Fenton J D 1985 A fifth-order Stokes theory for steady waves *J. Waterways, Port, Coastal Ocean Eng. ASCE* **3** 216–34

Gerstner F J 1802 Theorie de Wellen *Abh. D. K. Bohm. Ges. Wiss.* (Reprinted in *Ann. Phys.* 32 412–40)

Henry D 2008 On Gerstner's water wave *J. Nonlinear Math. Phys.* **15** 87–95

Henry D 2009 Steady periodic flow induced by the Korteweg–de Vries equation *Wave Motion* **46** 403–11

Johnson R S 1997 *A Modern Introduction to the Mathematical Theory of Water Waves* (Cambridge: Cambridge University Press)

Lamb H 1932 *Hydrodynamics* 6th edn (Cambridge: Cambridge University Press)

Longuet-Higgins M S 1986 Eulerian and Lagrangian aspects of surface waves *J. Fluid Mech.* **173** 683–707

Longuet-Higgins M S 1987 Lagrangian moments and mass transport in Stokes waves *J. Fluid Mech.* **179** 547–55

Mei C C 1983 *The Applied Dynamics of Ocean Surface Waves* (New York: Wiley)

Miche A 1944 Mouvements ondulatoires de la mer en profondeur constante ou décroissante *Ann. Ponts Chaussées* pp 25–78, 131–64, 270–92, 369–406

Naciri M and Mei C C 1993 Evolution of short gravity waves on long gravity waves *Phys. Fluids.* A **5** 1869–78

Piedra-Cueva I 1995 Drift velocity of spatially decaying waves in a two-layer viscous system *J. Fluid Mech.* **229** 217–39

Pierson W J 1962 Perturbation analysis of the Navier–Stokes equations in Lagrangian form with selected linear solution *J. Geophy. Res.* **67** 3151–60

Rankine W J M 1863 On the exact form of waves near the surface of deep water *Phil. Trans. R. Soc.* A **153** 127–38

Reinecker M M and Fenton J D 1981 A Fourier approximation method for steady water waves *J. Fluid Mech.* **104** 119–37

Sanderson B 1985 A Lagrangian solution for internal waves *J. Fluid Mech.* **152** 191–202

Skjelbreia L and Hendrickson J 1960 Fifth order gravity wave theory *Proc. 7th Coastal Engineering Conf. ASCE* pp 184–96

Stokes G G 1847 On the theory of oscillatory waves *Trans. Camb. Phil. Soc.* **8** 441–55

Yakubovich E I and Zenkovich D A 2001 Matrix approach to Lagrangian fluid dynamics *J. Fluid Mech.* **443** 167–96